Molecular Therapy
Nucleic Acids
Original Article

Nanoparticle Delivery of Anti-inflammatory LNA Oligonucleotides Prevents Airway Inflammation in a HDM Model of Asthma

Sabrina C. Ramelli,[1] Brian S. Comer,[1] Jared M. McLendon,[1] Lydia L. Sandy,[1] Andrew P. Ferretti,[2] Robert Barrington,[2] Jeff Sparks,[3] Majed Matar,[3] Jason Fewell,[3] and William T. Gerthoffer[1,2]

[1]Department of Biochemistry and Molecular Biology, University of South Alabama, Mobile, AL, USA; [2]Department of Microbiology and Immunology, University of South Alabama, Mobile, AL, USA; [3]Celsion Corporation, 601 Genome Way, Huntsville, AL, USA

To address the problem of poor asthma control due to drug resistance, an antisense oligonucleotide complementary to mmu-miR-145a-5p (antimiR-145) was tested in a house dust mite mouse model of mild/moderate asthma. miR-145 was targeted to reduce inflammation, regulate epithelial-mesenchymal transitions, and promote differentiation of structural cells. In addition, several chemical variations of a nontargeting oligonucleotide were tested to define sequence-dependent effects of the miRNA antagonist. After intravenous administration, oligonucleotides complexed with a pegylated cationic lipid nanoparticle distributed to most cells in the lung parenchyma but were not present in smooth muscle or the mucosal epithelium of the upper airways. Treatment with antimiR-145 and a nontargeting oligonucleotide both reduced eosinophilia, reduced obstructive airway remodeling, reduced mucosal metaplasia, and reduced CD68 immunoreactivity. Poly(A) RNA-seq verified that antimiR-145 increased levels of many miR-145 target transcripts. Genes upregulated in human asthma and the mouse model of asthma were downregulated by oligonucleotide treatments. However, both oligonucleotides significantly upregulated many genes of interferon signaling pathways. These results establish effective lung delivery and efficacy of locked nucleic acid/DNA oligonucleotides administered intravenously, and suggest that some of the beneficial effects of oligonucleotide therapy of lung inflammation may be due to normalization of interferon response pathways.

INTRODUCTION

New classes of drugs to treat asthmatics who are resistant to corticosteroids or beta agonists are urgently needed. Biologic drugs have emerged that are effective in many, but not all, subsets of asthma patients.[1–3] Immunotherapy approaches provide some benefit but still do not halt or reverse the remodeling of structural cells in severe asthmatics. Because asthma is a genetically complex, multifactorial syndrome with multiple endotypes, a therapy that targets multiple protein mediators might ultimately be more beneficial to patients whose condition is not controlled by standard therapies. Ideal new drugs would be long-acting treatments that inhibit inflammation, prevent and reverse airway remodeling, and promote bronchodilation. Our working hypothesis was that antagonizing the function of pro-inflammatory microRNAs (miRNAs) with miRNA antagonists could have both anti-inflammatory and disease-modifying anti-remodeling effects. This seems likely, because miRNAs regulate immune and structural lung cell phenotypes by targeting and regulating multi-protein networks.[4]

miRNAs that control lung cell lifespan, differentiation, inflammation, fibrosis, and smooth muscle contraction are logical targets.[5–7] First-generation antisense oligonucleotide (ASO) therapies delivered by inhalation targeted mRNAs coding for single proteins, including interleukin (IL)-5,[8] tumor necrosis factor alpha (TNF-α),[9] STAT6,[10] and p38 mitogen-activated protein (MAP) kinases.[11] The modest success reported in these studies suggests that other approaches are needed. To overcome the limitations of targeting single proteins, second-generation ASO agents have targeted miRNA regulatory networks.[4,12–14] In the present study, we targeted miR-145 because it has been proven beneficial in a mouse model of asthma.[15] In addition, we investigated several nontargeting oligonucleotides to define any sequence-dependent and -independent effects of locked nucleic acid (LNA)/DNA oligonucleotides. In all studies, the oligonucleotides were complexed to a cationic lipid nanoparticle and delivered intravenously to circumvent barriers common to aerosol delivery of oligonucleotides, which include mucus plugging of the airways and low drug levels reaching distal airways.

The novel pegylated cationic lipid nanoparticle used in this study was found previously to yield high oligonucleotide levels in pulmonary vascular endothelial cells (TheraSilence, Celsion, Huntsville, AL, USA).[16–18] In the prior studies, small interfering RNAs

Received 20 February 2019; accepted 9 December 2019;
https://doi.org/10.1016/j.omtn.2019.12.033.

Present address: Department of Pharmacology, School of Medicine, University of Nevada, Reno, Reno, NV 89557, USA

Correspondence: William T. Gerthoffer, PhD, Department of Biochemistry and Molecular Biology, University of South Alabama, Mobile, AL, USA.
E-mail: wgerthoffer@med.unr.edu

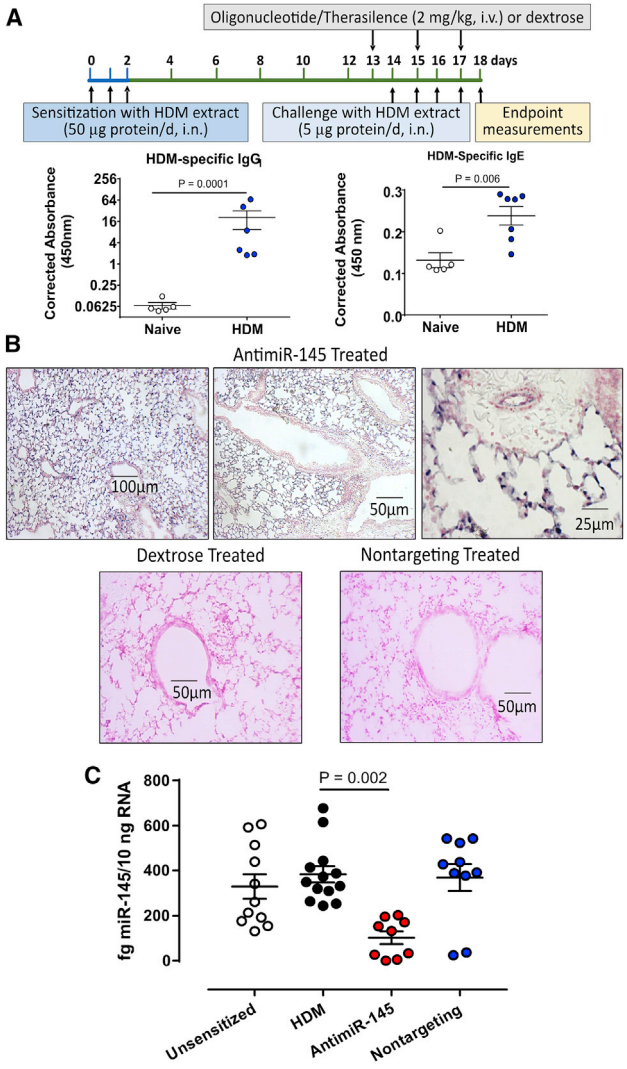

Figure 1. Delivery of antimiR-145 ASO to Lung Tissues in a HDM Model of Mild/Moderate Asthma

(A) The HDM asthma model was adapted from Collison et al.[15] The protocol had 3 phases: (1) Three-day sensitization beginning on day 0 to promote atopy; (2) three doses of 2 mg/kg antimiR-145 or solvent control (5% dextrose in 0.9% saline) every other day beginning on day 13; and (3) four daily challenges with HDM extracts beginning on day 14. On day 18, blood was collected for antibody assays, bronchioalveolar lavage fluids were collected for immune cell analysis, and lung tissue was collected for histologic analysis and extraction of RNA and protein. Naive (unsensitized) animals were age matched and treated with saline instead of HDM extract. Serum HDM-specific serum IgG_1 and IgE were significantly increased after allergic sensitization. Total IgG and IgE were not significantly changed after HDM sensitization and challenge (data not shown). Data are mean ± SEM; Student's t test; n = 5–7. (B) The distribution of antimiR-145 in lung tissue was determined by ISH. Sections of the left lung lobe of HDM-sensitized mice were probed with a DIG-labeled LNA/DNA oligonucleotide complementary to antimiR-145. Positive tissues were visualized with anti-DIG antibodies conjugated to AP and were counterstained with Nuclear Fast Red. Sections from a sensitized mouse treated with antimiR-145/TheraSilence are shown at 10×, 20×, and 40× magnifications (top panels). A lung section from a dextrose-treated, HDM-sensitized mouse (lower left panel) was negative, as was a section from a sensitized mouse treated with a nontargeting oligonucleotide (lower right panel). Images are representative examples of sections from n = 9–18 mice per treatment group. (C) Treatment with antimiR-145 reduced mature miR-145 levels in lung. qRT-PCR of miRNA-145 was performed on total RNA from mouse lungs. Sets of mice were unsensitized, sensitized with HDM and treated with dextrose (HDM), sensitized and treated with antimiR-145, or sensitized and treated with nontargeting control oligonucleotide. Statistical analysis was performed by one-way ANOVA with Dunnett's post hoc test using the HDM-sensitized treatment as the reference group; n = 9–13.

(siRNAs) and ASOs were retained in the lung, with no significant toxicity in mice or rats.[16,18] Effective knockdown of target proteins was demonstrated,[16,17] and a therapeutic effect was achieved in a rat model of severe pulmonary hypertension.[18] We extended these initial findings by testing for anti-inflammatory and anti-remodeling effects of a miR-145-targeting ASO and nontargeting oligonucleotides in a house dust-mite (HDM) model of mild/moderate Th2-high asthma. The miR-145 antagonist was delivered effectively to lower airways and altered expression of miR-145 target transcripts and asthma-related genes. However, much of the anti-inflammatory effect appeared to be due to significant, important anti-inflammatory effects of the LNA/DNA phosphorothioate oligonucleotide structure. We suggest that there are multiple structural features of therapeutic oligonucleotides that contribute beneficial effects in the asthma model. A preliminary report of this work appeared in a published abstract.[19]

RESULTS

Lung Delivery of AntimiR-145

Achieving effective delivery of oligonucleotides to the lungs is a major challenge in developing successful RNAi-based therapy of asthma. To verify that TheraSilence is an effective delivery vehicle, we performed *in situ* hybridization (ISH). Mice were sensitized and challenged with HDM extracts to elicit atopic inflammation and lung remodeling (Figure 1A). HDM-specific immunoglobulin (Ig) E increased after sensitization, consistent with successful atopic inflammation of the lung. Formalin-fixed lung sections from HDM-sensitized mice were probed with a digoxigenin (DIG)-labeled probe complementary to antimiR-145 (Figure 1B). AntimiR-145 was most abundant in the parenchyma, airway epithelium, and pulmonary vascular endothelium but did not accumulate in smooth muscle or mucosa of large airways (>300-µm diameter). To verify the sequence specificity of the anitmiR-145 probe, we assayed lung sections from HDM-sensitized animals treated with dextrose and HDM-sensitized animals treated with a nontargeting oligonucleotide (Figure 1B, lower panels). Both control treatments proved to be negative. ISH was also conducted to determine the distribution of a nontargeting LNA/DNA oligonucleotide. Lungs from sensitized animals treated with the nontargeting oligonucleotide were positive and showed the same pattern of deposition as antimiR-145 (data not shown). Lungs from animals treated with antimiR-145 showed no staining for the nontargeting oligo probe. The same distribution pattern was observed for both oligonucleotides, demonstrating that distribution within the lung was not sequence dependent.

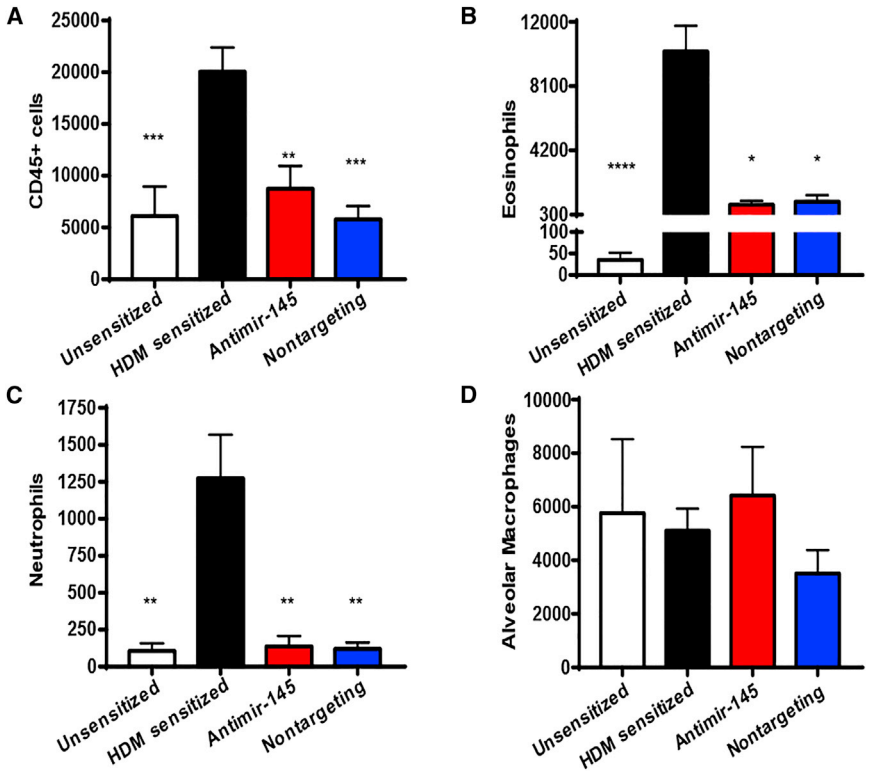

Figure 2. AntimiR-145 Treatment Reduces Immune Cells in BALF

Cells from BAL fluid (BALF) were counted by analytical flow cytometry. (A) The total number of CD45+ cells is shown. (B–D) Other panels show effects on eosinophils (B), neutrophils (C), and alveolar macrophages (D). Statistical hypothesis testing was performed with Kruskal-Wallis ANOVA and Dunn's post hoc test using counts of HDM-sensitized treated animals as the reference. *$p < 0.05$; **$p < 0.01$; ***$p < 0.001$. n = 10–18.

AntimiR-145 Treatment Reduces Endogenous mmu-miR-145a-5p Levels

miRNA-145 directly represses expression of many experimentally validated targets, some of which contribute to lung remodeling following allergic sensitization (Table S4)[65–75]. Genes regulating smooth muscle hypertrophy, epithelial-to-mesenchymal transitions, and stem cell maturation are all potential targets for therapies designed to halt, or even reverse, airway remodeling. We predicted that treating sensitized mice with antimiR-145 would antagonize the function of native miR-145-5p, thus upregulating abundance of miR-145 target mRNAs to prevent lung remodeling. To test this hypothesis, we first determined whether antimiR-145 knocked down mature miR-145-5p levels. miR-145 levels were significantly reduced in HDM-sensitized mice treated with antimiR-145 (Figure 1C). The nontargeting oligonucleotide did not significantly affect the mean levels of mature miR-145 (Figure 1C).

Oligonucleotide Effects on Inflammation in HDM-Sensitized Mice

To establish the efficacy of antimiR-145 in preventing allergic lung inflammation, the effects on immune cell infiltration into bronchiolar alveolar lavage (BAL) fluid (BALF) were determined in four sets of mice: unsensitized, HDM-sensitized treated with dextrose, HDM-sensitized treated with antimiR-145, and HDM-sensitized treated with nontargeting oligonucleotide. The number of $CD45^+$ hematopoietic cells in BALF was reduced by treatment with antimiR-145 compared to HDM-sensitized animals (Figure 2A). Both eosinophil and neutrophil counts increased in HDM-sensitized mice and were significantly reduced by treatment with antimiR-145 (Figures 2B and 2C). The number of alveolar macrophages was not significantly changed (Figure 2D).

Lung inflammation in asthma also leads to immune cell deposition around the airways and pulmonary vessels. Tissue immune cell infiltration was assessed quantitatively in hematoxylin and eosin (H&E)-stained and formalin-fixed (at 25 cm H_2O pressure), paraffin-embedded (FFPE) lung slices. The size and cross-sectional areas of hematoxylin-stained bronchus-associated lymphoid tissues (BALTs) were measured using Fiji (ImageJ). De-identified images were evaluated by an investigator blinded to the treatment groups. Figure 3A shows representative images of lung sections from unsensitized, HDM-sensitized, and oligonucleotide-treated mice. HDM-sensitized lungs contained increased BALTs in all animals. Treatment with antimiR-145 significantly reduced the volume density of inflamed area (Figure 3A), which could be the result of fewer inflamed sites, smaller size of inflamed sites, or both. Counting the number of inflamed sites revealed a significant reduction in the number of sites but no difference in the size of the inflamed sites (data not shown). Again, we were surprised that the nontargeting control oligonucleotide had significant inhibitory effects on tissue inflammation similar to that of the antimiR-145 oligonucleotide (Figure 3A). Together with the results on immune cells in BAL, these data show that antimiR-145 treatment reduced inflammation in HDM-sensitized mice. However, the results also raise a question as to how much of the anti-inflammatory effect was due to sequence-specific effects on miR-145 targets.

During the immune response in asthma, monocytes are recruited to sites of inflammation where they differentiate into tissue macrophages that can embed in the interstitium or remain in the alveolar space along with alveolar macrophages. To determine whether oligonucleotide therapy could reduce tissue macrophage deposition, FFPE lung sections were stained with anti-CD68 antibodies. The number of $CD68^+$ tissue macrophages (Figure 3B, brown cells) in sensitized mice treated with antimiR-145 was reduced compared to that in mice treated with dextrose. Treatment with antimiR-145

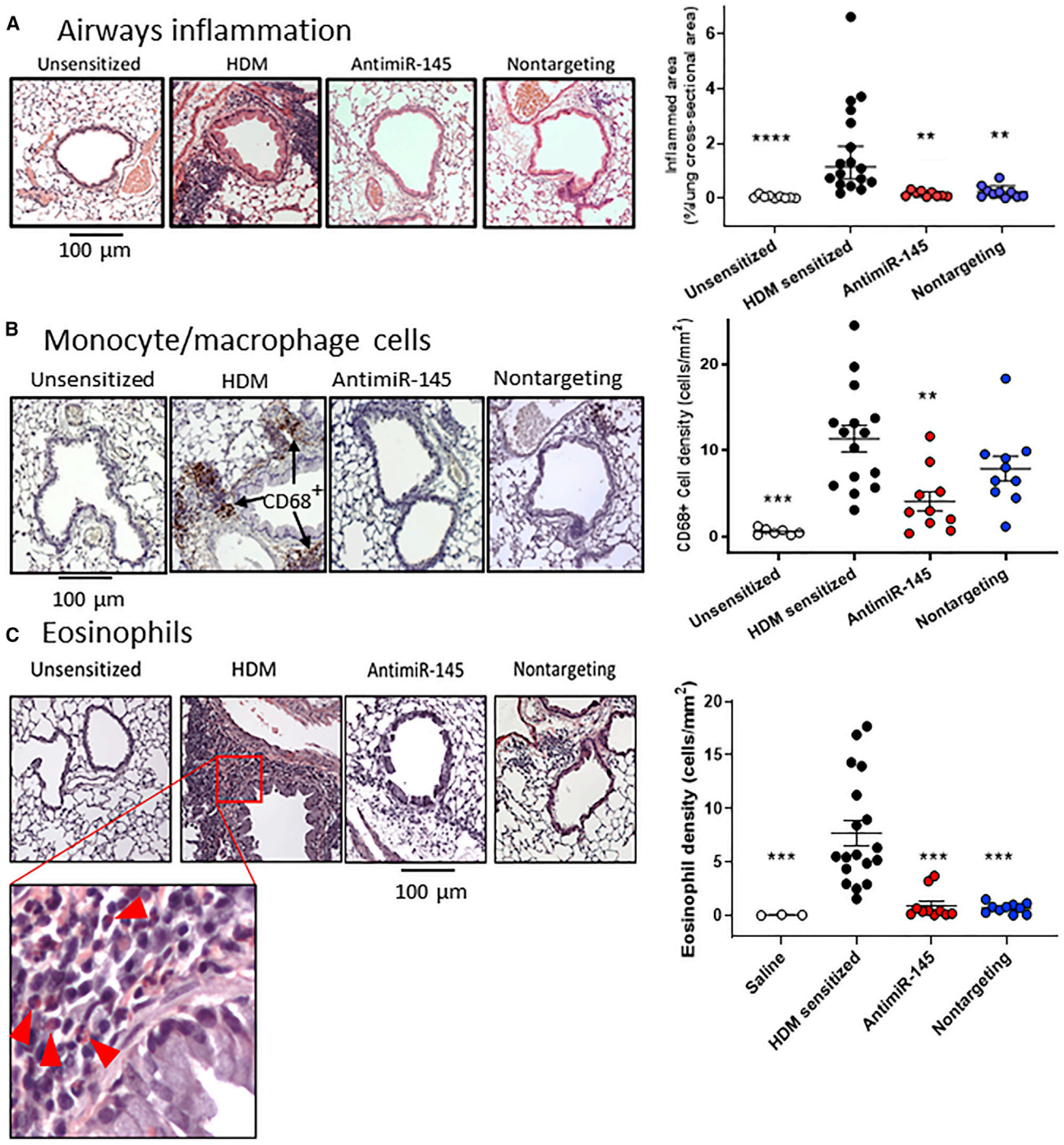

Figure 3. AntimiR-145 Treatment Reduces Lung Tissue Inflammation

(A) FFPE lung sections were stained with H&E to identify sites of inflammation (purple clusters). Representative micrographs for each treatment group. Volume density was calculated by measuring areas of inflammation and normalizing to lung lobe cross-sectional area. Data are indicated as geometric mean ± 95% CI. Statistical hypothesis testing was performed using Kruskal-Wallis ANOVA and Dunn's post hoc test, with the HDM-sensitized treatment as the reference group. **$p < 0.005$; ***$p < 0.001$. n = 9–17. (B) Treatment with antimiR-145 reduces CD68+ tissue macrophages. FFPE lung lobe sections were stained with anti-CD68 antibody and counterstained with hematoxylin to identify tissue macrophages (brown). A representative micrograph for each treatment group is shown. CD68+ cells were counted in images covering an entire lung section for

(legend continued on next page)

significantly reduced the density of CD68+ tissue macrophages (cells per square millimeter), but the nontargeting oligonucleotide did not produce a statistically significant effect (Figure 3B, right panel). These data indicate that antimiR-145 treatment produces a sequence-dependent reduction in the number of tissue macrophages.

In addition to monocytes and macrophages, eosinophils are also known to be recruited to sites of lung inflammation in humans and in mouse models of asthma. To determine whether the oligonucleotides have an anti-eosinophilic effects, lung sections were stained with Sirius red (Figure 3C). The number of eosinophils in the tissue was significantly reduced by both the antimiR-145 and nontargeting oligonucleotides. These data indicate that both antimiR-145 and the nontargeting oligonucleotide had an anti-eosinophil effect that was not entirely due to the sequence of antimiR-145.

Oligonucleotide Treatment Reduces Mucosal Remodeling in HDM-Sensitized Mice

Airway obstruction in mild-to-moderate asthma is due, in part, to epithelial damage with goblet cell hyperplasia and increased mucus secretion, leading to mucus plugging of the small airways. These hallmarks are recapitulated in the HDM mouse model of Th2 high asthma (Figure 4A). To assess mucosal remodeling and mucin production, FFPE lung tissues were stained by periodic acid Schiff (PAS) stain. The volume density of PAS staining was quantified by point count morphometry by an investigator blinded to the treatment groups. Lungs of all HDM-sensitized mice stained positively in airways with a diameter larger than 100 μm in contrast to unsensitized animals, which were all negative. There was an obvious reduction in PAS staining in both antimiR-145-treated and nontargeting-oligonucleotide-treated mice compared to dextrose-treated mice (Figure 4A, right panels). We also wanted to determine the size of the airways where mucus secretion was induced, because mice normally produce mucus only in the trachea and primary bronchi.[20] There was no PAS staining in airways with a diameter less than 100 μm in any treatment group. However, in airways with diameters of 100–300 μm and 300–600 μm, HDM sensitization increased PAS staining, which was significantly reduced by both oligonucleotide treatments (Figures 3B and 3C). These data confirm the findings of prior studies reporting increased mucin expression deeper in the airway tree in HDM-sensitized mice compared to unsensitized mice.[21] The data also show that the therapeutic benefit of oligonucleotide therapy was most pronounced in airways with a diameter of 100 to 600 μm.

Pathway Analysis of Oligonucleotide-Treated, HDM-Sensitized Mice

To determine whether antimiR-145 blocked the functional effects of miR-145, we assessed the expression of a set of predicted mmu-miR-145a-5p targets (Table S5). Using DESeq2 and gene set enrichment analysis (GSEA), we found that allergic sensitization reduced the expression of 91 predicted miR-145 target genes with miRNA target gene (miTG) scores >0.7[22] (Figure 5A). We then compared the expression of miR-145 targets in HDM-sensitized animals treated with antimiR-145 versus animals that were HDM sensitized with the nontargeting oligonucleotide. Treatment with antimiR-145 increased the expression of 75 miR-145 targets (Figure 5B). In contrast, the nontargeting oligonucleotide did not significantly alter expression of miR-145 targets in sensitized mice (Figure 5B). Therefore, distribution of antimiR-145 oligonucleotide throughout the lung resulted in the upregulation of miR-145a target transcripts, consistent with antimiR-145 inhibiting native miR-145 function *in vivo*.

Allergic inflammation in asthma results in the upregulation of multiple protein mediators and signaling pathway components. Two Th2 cytokines, IL-5 and IL-13, were found previously to be reduced in cultured Th2 cells from antimiR-145-treated HDM-sensitized mice.[15] We extended this analysis by determining whether the differences we found in inflammation and mucosal remodeling correlated with whole-lung transcriptomics. Poly(A) RNA sequencing (RNA-seq) and differential expression analysis were used to detect differentially expressed transcripts at the gene level. RNA-seq data have been deposited in NCBI's Gene Expression Omnibus and are accessible with the accession number GEO: GSE126610.

Many cytokines and chemokines that are upregulated in humans with asthma and in mouse models of asthma were downregulated by antimiR-145 treatment (Figure 6A). PCR validation studies verified that IL-4 and IL-17a were upregulated in sensitized lungs and that antimiR-145 significantly reduced whole-lung IL-4 levels (Figure S1). Whole-lung expression of IL-13 and IL-5 was not altered by HDM sensitization, nor did antimiR-145 alter IL-13 or IL-5 gene expression in contrast to the prior study of these cytokines in Th2 cells from lymph nodes.[15] This highlights an important difference in the effect of HDM sensitization on primary lymph tissue versus gene expression in whole lung, where hematopoietic cells, airway epithelial cells, and vascular endothelial and structural cells (fibroblasts and smooth muscle) all contribute to gene expression patterns.

Biomarker studies have revealed sets of lung transcripts and proteins associated with asthma.[23,24] Many of the same genes upregulated in asthma are also upregulated in a short-term HDM model of asthma.[25] In the present study, several established biomarkers of human type II inflammation (Clca1, IL-6, periostin, and IL-13)[26,27] were significantly upregulated by HDM sensitization, and all but periostin were significantly downregulated after treatment with antimiR-145 (Figure 6B).

The nontargeting oligonucleotide also downregulated asthma-related gene sets (Figure 6A, blue bars) and asthma biomarkers (Figure 6B).

each mouse. The number of CD68+ cells was normalized to lung lobe cross-sectional area. Statistical hypothesis testing was performed with Kruskal-Wallis ANOVA and Dunn's post hoc test. *$p < 0.05$; ***$p < 0.01$. n = 10–18. (C) Sirius red staining identifies eosinophils (bright pink with purple bilobular nucleus) at sites of lung inflammation. Eosinophils are indicated by red arrowheads in the enlarged inset. The number of eosinophils was counted in all fields of each lung section for each animal and normalized to lung lobe cross-sectional area. Statistical hypothesis testing was performed by Kruskal-Wallis ANOVA and Dunn's post hoc test; ***$p < 0.001$. n = 3–18.

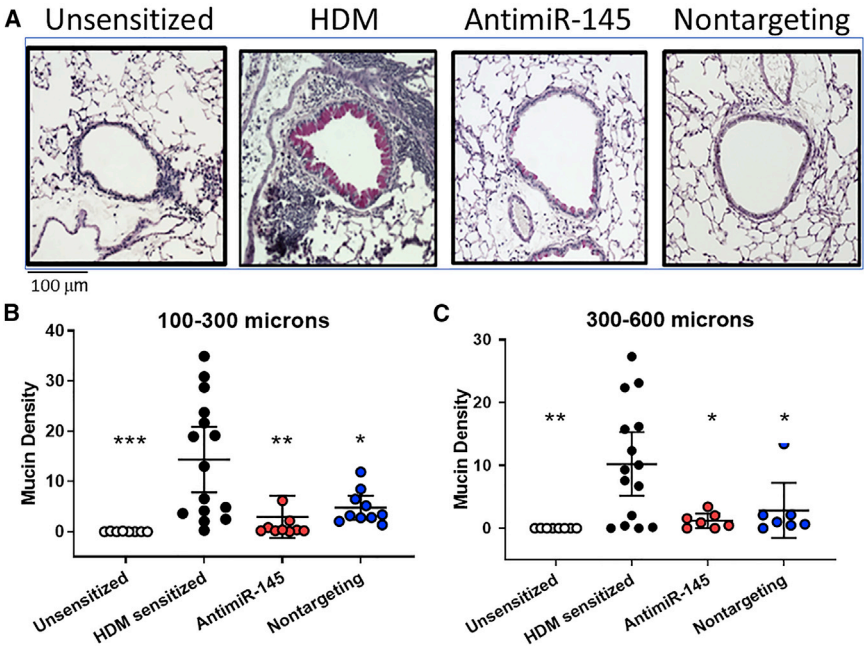

Figure 4. Oligonucleotide Treatments Reduce Mucosal Metaplasia

FFPE lung sections were stained with Periodic Acid Schiff stain to identify mucus-producing cells (magenta). (A) A representative micrograph for each treatment group illustrates staining in airways with a diameter of 150–200 μm. (B and C) Mucin density was measured by a point count method, and results were stratified by airway diameter: <100 μm (data not shown), 100–300 μm (B), 300–600 μm (C), and airways >600 μm (data not shown). Significant treatment effects were observed in airways with diameters between 100 and 600 μm. Statistical hypothesis testing was performed with Kruskal-Wallis ANOVA and Dunn's post hoc test comparing all treatments to HDM-sensitized animals. *$p < 0.05$; **$p < 0.01$; ***$p < 0.005$. n = 10–18 mice.

More detailed analysis of GSEA results showed that both oligonucleotides also modified the expression of gene sets related to immune response, tissue architecture, and metabolism (Figure S2). These genes code for proteins for interferon signaling, Notch signaling, Myc targets, targets of the E2F transcription factor, MTOR1C signaling, and oxidative phosphorylation. However, the effects of both oligonucleotides were not identical. Treatment with antimiR-145 produced significant downregulation of EMT, IL2 signaling, and metabolic pathways that were unaffected by the nontargeting oligonucleotide. In addition, the nontargeting oligonucleotide had no significant effect on the set of mmu-miR-145a-5p targets in HDM-sensitized mice in contrast to antimir-145 (Figure 5). This suggests that there are multiple molecular mechanisms responsible for the anti-inflammatory and anti-remodeling effects of oligonucleotide delivered with TheraSilence nanoparticles.

Since both antimiR-145 and the nontargeting oligonucleotide reduced expression of inflammatory signaling pathways, we surveyed a number of other gene sets relevant to lung remodeling in asthma, including glucocorticoid signaling,[28] genes that contribute to pulmonary fibrosis,[29] and genes that establish the smooth muscle contractile phenotype[30–32] (Figure 6A). HDM sensitization significantly upregulated the smooth muscle gene set but did not significantly affect a liver glucocorticoid receptor signaling gene set or a pulmonary fibrosis-related gene set. Although there was a consistent trend to reduce expression of each gene set, antimiR-145 treatment did not significantly affect expression of these gene sets in HDM-sensitized mice.

DNA oligonucleotides, including DNA/LNA mixmers used in this study, can function as damage-associated molecular pattern (DAMP) molecules, suggesting that some effects of antimir-145 might be unrelated to antagonism of miR-145 functions. Therefore, we also tested a nontargeting LNA/DNA oligonucleotide designed to not hybridize to any known miRNA binding site in mammalian genomes. We were surprised to find that the nontargeting oligonucleotide also downregulated cytokine and chemokine gene sets but to a lesser extent than antimiR-145 did (Figure 6A). One of the more intriguing findings was that both interferon alpha and gamma signaling pathway genes were upregulated significantly by both antimiR-145 and oligonucleotide treatments (Figure 7; Figure S2). Neither type 1 or type 2 interferon transcripts themselves were affected by oligonucleotide therapy, but many of the downstream signaling pathway components were upregulated, including transcripts in the cellular innate immune response (Adar, Oasl2, Il15, Fas, and Casp1). The effect was apparently not sequence specific and, thus, not entirely due to functional antagonism of native miR-145. Rather, there may be a more general effect of LNA/DNA oligonucleotides to upregulate the innate immune response in lung cells. This effect is theoretically desirable in asthma therapy, because interferon response pathways are blunted in some asthmatics, particularly during asthma exacerbations due to lung infections.[33]

Oligonucleotide Effects on Remodeling in HDM-Sensitized Mice

The significant anti-inflammatory and anti-mucosal remodeling effects of the nontargeting oligonucleotide are some of the more interesting outcomes of the study. The same nontargeting oligonucleotide had previously been shown to have minimal effect on lung structure in an *in vivo* study of pulmonary arterial hypertension.[18] However, in the setting of allergic sensitization of the lung, the nontargeting oligonucleotide was not a useful negative control. In fact, it showed efficacy as an anti-inflammatory "drug," despite being designed to lack sequence complementary to mammalian miRNA targets. This suggests that a structural feature other than the nucleotide sequence was responsible for anti-remodeling activity.

The nontargeting oligonucleotide is a 15-nt LNA/DNA mixmer with a phosphorothioate backbone (5′-ACGTCTATACGCCCA-3′). We tested the hypotheses that the apparent anti-inflammatory effects

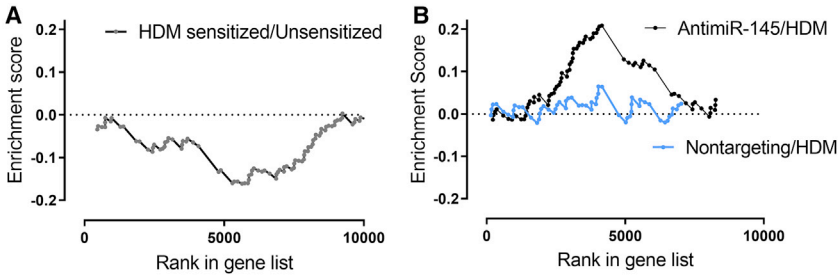

Figure 5. AntimiR-145 Upregulates mmu-miR-145a-5p Targets in HDM-Sensitized Mice

Deseq2 analysis followed by gene set enrichment analysis (GSEA) was used to assess sequence-dependent effects of antimir-145 on mmu-miR-145a-5p target genes. Mouse miR-145a-5p targets were identified *in silico* (DIANA-microT-CDS).[22] (A) Expression of miR-145 target genes is reduced by HDM sensitization when compared to unsensitized controls. NES = −1.9, $p < 0.01$. n = 5 for unsensitized mice, and n = 10 for HDM-sensitized mice. (B) Expression of miR-145 target genes in lungs of HDM-sensitized mice is enhanced by antimiR-145 treatment (black circles); NES = 2.1, $p < 0.001$. n = 10 for HDM-sensitized and HDM-sensitized plus antimir-145 groups. A nontargeting LNA/DNA oligonucleotide did not significantly alter the expression of miR-145 target genes in HDM-sensitized mice (blue circles). n = 5 for nontargeting-oligonucleotide-treated mice.

may due to pharmacological effects of the phosphorothioate backbone, the 2′-O, 4’-C methylene bridge on the ribofuranose ring of LNA bases, or both. Some LNA/DNA mixmers with phosphorothioate backbones can act as toll-like receptor (TLR)7 and TLR8 antagonists.[34] Nanoparticles with lipid membrane structures are avidly taken up by dendritic cells and can exert an immunosuppressive effect that includes decreased myosin heavy chain (MHC), TNF-α, interferon gamma, IL-12 p70, and IL-1β expression.[35] Therefore, to define the relative contributions of the phosphorothioate backbone, the locked nucleic acid residues, and the lipid nanoparticle, two additional nontargeting oligonucleotides were tested in HDM-sensitized mice. Both had the same sequence as the LNA/DNA nontargeting oligonucleotide but different backbones: DNA oligonucleotide, 5′-ACGTCTATACGCCCA-3′; and phosphorothioate control (PS oligonucleotide), 5′-A*C*G*T*C*T*A*T*A*C*G*C*C*C*A-3′. The asterisk indicates phosphorothioate linkages.

The effects of the modified nontargeting oligonucleotides were assessed on immune cell infiltration in BALFs. The total number of CD45+ hematopoietic cells decreased significantly after treatment with the nontargeting oligonucleotide and the PS oligonucleotide but not the DNA oligonucleotide (Figure 8A). Most of the effect was due to decreased eosinophil and neutrophil counts (Figures 8B and 8C). The number of alveolar macrophages was not reduced by any oligonucleotide (Figure 8D). Tissue inflammation was also assessed and quantified by inflammation scoring of H&E-stained lung sections (Figure 8E). There was a significant reduction in the volume density of inflamed sites in HDM-sensitized mice treated with nontargeting LNA/DNA oligonucleotide but not the PS or DNA oligonucleotide (Figures 8E and 8F). Effects of TheraSilence nanoparticles alone were also assessed on tissue inflammation (Figure S3). We found no significant effect on volume density of lung inflammatory cells. These data indicate that the PS and DNA oligonucleotides do not consistently inhibit tissue inflammation and are less effective anti-inflammatory molecules compared to the LNA-modified nontargeting oligonucleotide with a phosphorothioate backbone.

DISCUSSION

Inhaled corticosteroids and beta agonists are effective in treating asthma in about 90% of asthma patients.[36,37] The remaining 5%–10% of asthmatics are steroid resistant and, in some cases, also resistant to beta agonists, accounting for about 50% of the medical cost of asthma therapy.[36,38] Important new biologic therapies have been developed to address this problem. However, one disadvantage of antibody therapies is that each drug targets one molecule. In some cases, the biologics are effective only in a limited subset of uncontrolled asthmatics. An alternative approach is to target multiple proteins in multiple pathways that contribute to disease, a strategy termed polypharmacology. Although most often applied to small-molecule drug development, the concept can be extended to the development of miRNA-based drugs. Successful oligonucleotide drugs would modify multiple signaling pathways that are important in inflammation but, unlike corticosteroids, would not be limited by steroid-resistance mechanisms. In addition, ideal new treatments would prevent or reverse airway wall remodeling in ways that corticosteroids do not. We reasoned that a polypharmacology approach might be effective because asthma is a complex syndrome caused by multiple predisposing gene variants, multiple cell types, and multiple inflammatory molecules.[39–41] miRNAs are logical drug targets, because they regulate the abundance of multiple proteins in the networks of coordinately expressed genes. Numerous miRNAs and their downstream protein networks are dysregulated in complex diseases, including asthma and animal models of asthma.[5,42–44] By antagonizing the function of one or more of these miRNAs, it might be possible to block inflammation and reverse airway remodeling, thus producing a long-lasting prevention of airway hyperreactivity. Two important problems must be overcome to achieve these goals. Effective, nontoxic delivery methods must be used, and the new agents must effectively modulate miRNA target expression leading to the desired therapeutic response.

As an early step toward oligonucleotide-based therapy of asthma, we investigated the potential therapeutic effects of a miR-145 antagonist. miR-145 abundance is increased in asthma[45] and is known to regulate smooth muscle hypertrophy,[46,47] fibrosis,[48] and lung inflammation.[46,49] By antagonizing the deleterious effects of miR-145, the asthmatic airway might then be repaired by normal tissue remodeling mechanisms. To inhibit miR-145 function, an antisense LNA/DNA oligonucleotide was delivered effectively using a lipid nanoparticle with an attractive lung-directed pharmacokinetic profile. TheraSilence

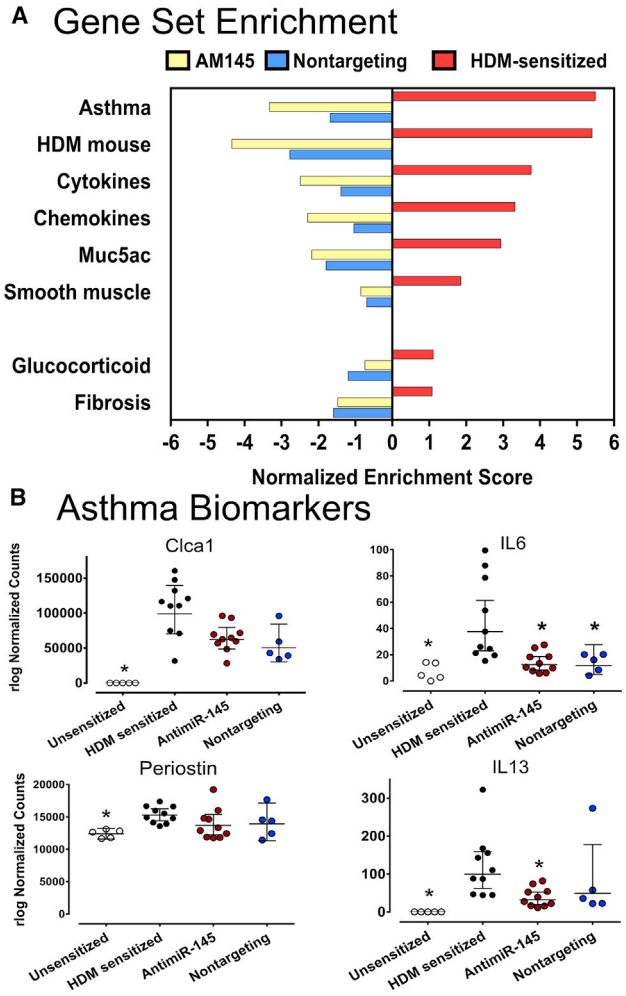

Figure 6. HDM-Enhanced Expression of Asthma-Related Gene Expression Is Antagonized by antimiR-145 and a Nontargeting Oligonucleotide

(A) Gene set enrichment analysis (GSEA) was performed on poly A RNA-seq data from whole lung samples. Left panel, asthma-related gene sets were compared between HDM-sensitized mice and sensitized mice treated with AM145 (blue bars). Asthma-related genes were also compared in HDM-sensitized mice versus sensitized mice treated with non-targeting oligonucleotide (yellow bars). Right panel, asthma-related gene expression in HDM-sensitized mice compared to age-matched unsensitized control mice (red bars). Normalized enrichment scores were significant for all gene sets; $p < 0.001$, n = 5-10. (B) Expression of human asthma biomarkers was assessed using rlog normalized counts from DESeq2. Data are expressed as mean counts +/− 95% confidence intervals; * − $p < 0.05$, One-way ANOVA on log transformed data, Dunn's post hoc test with HDM-sensitized treatment as the reference group, n = 5-10.

is a cationic lipid nanoparticle formulation that concentrates siRNA and small oligonucleotides in lung tissue.[16–18] siRNAs delivered by TheraSilence effectively knocked down caveolin and VEGF with effects that lasted significantly longer than in liver and kidney.[16] The siRNAs were retained for a sustained time (>48 h) and had biological function and activity for a minimum of 10 days after injection of a single dose. We took advantage of this favorable pharmacokinetic profile to compare the therapeutic effects of a miR-145 antagonist to that of several nontargeting oligonucleotides with varying structures in a HDM mouse model of mild to moderate asthma.

AntimiR-145 and a nontargeting LNA/DNA oligonucleotide both significantly reduced signs of lung inflammation by decreasing the number of eosinophils and CD68+ tissue macrophages (Figures 3 and 8). However, the nontargeting treatment only reduced the number of tissue eosinophils (Figure 8), suggesting that tissue macrophage reduction may be especially sensitive to the sequence of antimiR-145.

A prior study reported that intranasal administration of a naked 2′-O-methyl phosphoramadite miR-145 ASO formulation reduced mucosal metaplasia in sensitized mice.[15] In the present study, we found that delivering oligonucleotides from the blood compartment prevented the remodeling of secretory epithelial cells (Figure 4) and reduced the expression of genes that regulate Muc5ac production (Figure 6A; Table S5).[50] Both effects correlated with more normal airway epithelial structure and mucus secretion in HDM-sensitized mice.

The molecular bases of positive effects on BAL immune cells and lung inflammation were then explored by assaying differential gene expression in the lung. We used GSEA of poly(A) RNA-seq data to examine sets of coordinately expressed genes known to change during inflammation and asthma. We found that many genes associated with human asthma[23,24] were upregulated by HDM sensitization, as were genes upregulated in an HDM-sensitized mouse model of asthma (Figure 6).[25] We confirmed these prior observations and extended the list of differentially expressed genes to include pathways that mediate Muc5ac production,[50] the response to glucocorticoids,[28] and pulmonary fibrosis.[29] The GSEA results are consistent with BAL differential counts, histological measures, and immunoglobulin assay results, which show clear signs of Th2 high-allergic inflammation.

There were two aspects of remodeling that we could not recapitulate in the short-term HDM mouse model: airway smooth muscle hypertrophy and hyperplasia. The sensitization and challenge protocol we used did not elicit a significant thickening of the smooth muscle layer as identified by H&E staining, nor did HDM sensitization increase smooth muscle alpha actin immunohistochemical staining or contractile protein expression assessed by western blotting (Figure S4). HDM sensitization did upregulate the expression of a collection of genes that regulate the smooth muscle cell contractile phenotype (Figure 6A), but antimiR-145 did not alter expression of this gene set. The modest effects of HDM sensitization on lung smooth muscle are not unprecedented. Longer duration exposure to HDM or exposure to combinations of HDM and adjuvants or fungal allergens is required to reliably promote extensive remodeling of airway structure.

Allergic inflammation in asthma triggers the upregulation of multiple signaling proteins and signaling pathway components. Two

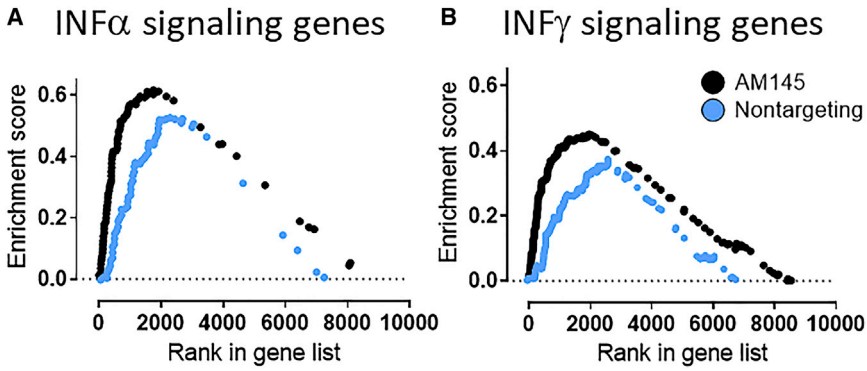

Figure 7. AntimiR-145 Upregulates Sets of Interferon-Regulated Genes

Gene set enrichment analysis (GSEA) was conducted to demonstrate differential gene expression in HDM-sensitized mice and HDM-sensitized mice treated with antimiR-145. HDM-sensitized mice served as the reference group for analysis of poly(A) RNA-seq data. A ranked set of differentially expressed genes (FDR < 0.2) was generated using DESeq2, and GSEA was performed using sets of interferon-regulated genes included in the Hallmark dataset of the MSigDB collection. (A) AntimiR-145 (black symbols) and nontargeting oligonucleotide (blue symbols) both significantly increased expression of most interferon-alpha-regulated genes ($p < 0.001$). (B) Treatments with antimiR-145 and nontargeting oligonucleotide also significantly enhanced interferon-beta-regulated genes ($p < 0.001$; $n = 10$ for each treatment).

cytokines that are expressed in Th2 high asthmatics, IL-5 and IL-13, were found previously to be reduced in cultured Th2 cells from antimiR-145-treated, HDM-sensitized mice.[15] We extended this analysis by determining whether the anti-inflammatory effects of antimiR-145 that we observed correlated with the abundance of cytokines, chemokines, and signaling pathway transcripts. GSEA revealed that many cytokine and chemokine genes known to be upregulated in asthma were downregulated by antimiR-145 treatment (Figure 6A). Again, we were surprised to find that the nontargeting oligonucleotide also downregulated the cytokine and chemokine gene sets (Figure 6A). This suggests that, although antimiR145 reduces miR-145a-5p expression (Figure 1C) and upregulates miR-145a-5p targets (Figure 5B), inhibition of inflammation is not entirely sequence dependent.

An interesting and potentially important finding that could explain the general anti-inflammatory effects of oligonucleotide delivery was that the interferon alpha and gamma pathways were upregulated significantly by both antimiR-145 and nontargeting oligonucleotide treatments (Figure 7). In patients with Th2 high asthma, some features of Th1 responses are blunted. Interferon gamma, a major anti-viral cytokine secreted during a Th1 response, is produced at low levels.[33] Th2 high asthma is associated with reduced production of interferons and increased risk of viral exacerbations.[33,51,52] By increasing some features of the Th1 response, oligonucleotide treatments might counteract the high Th2 immune response during allergic sensitization. While this is a provocative idea, the effect was clearly not entirely due to antimiR-145 sequence, because treatment with the nontargeting oligonucleotide also upregulated type I and type II interferon pathways (Figure 7). By increasing signaling through type I and type II interferons, both oligonucleotide treatments might be counteracting the Th2 immune response in mice. This could prove to be beneficial in human asthmatics and offer a potential alternative treatment that reduces asthma exacerbations.

One limitation of the present study is the absence of a detailed cellular mechanism or mechanisms to explain the positive therapeutic effect of oligonucleotides delivered by TheraSilence. The RNA-seq study used total RNA isolated from entire right lobes of the lung and not from cells of a single tissue type such as smooth muscle, fibroblasts, or airway epithelium. Subtle, but functionally significant changes in a single cell type might be below the detection threshold of our approach. Single cell RNA-seq analysis of dispersed lungs would be required to test this hypothesis. Another limitation is that antimiR-145 treatment may not be effective for all asthmatics because the molecular basis of asthma is highly variable. For example, our histological and gene expression analysis suggests that antimiR-145 may be effective for Th2 high asthmatics who have increased lung inflammation and mucosal metaplasia. Whether subjects with Th2 low/Th17 high phenotypes would be similarly responsive remains to be seen.

In summary, we demonstrated that LNA/DNA oligonucleotides formulated with TheraSilence were effective in preventing signs of allergic sensitization. Delivery of antimiR-145 to multiple cell types in the lung via the blood compartment reduced levels of endogenous miR-145, reduced immune cell infiltration, reduced inflammation, reduced mucosal metaplasia, and affected many gene sets associated with asthma and inflammation. Surprisingly, delivery of an LNA/DNA nontargeting oligonucleotide to the lung also reduced immune cell infiltration, reduced inflammation, reduced mucosal metaplasia, and affected many gene sets related to asthma and inflammation. A variety of LNA/DNA oligonucleotides might, therefore, have beneficial anti-inflammatory effects in the therapy of asthma; effects that are not due to targeting particular mRNAs or miRNAs. The beneficial effects on lung inflammation and mucosal remodeling occurred with no obvious adverse effects such as weight loss or lethargy, and in a study of rats with pulmonary hypertension, there were no effects of antimiR-145 on liver, kidney, or hematopoietic cell function as assessed by blood chemistry.[18] Although the dosing schedule was not fully optimized in the present study, the results suggest that a low-frequency, low-dose approach is sufficient to achieve significant anti-inflammatory and anti-remodeling results. Significant accumulation of oligonucleotides in cells of the lower airways and robust efficacy make

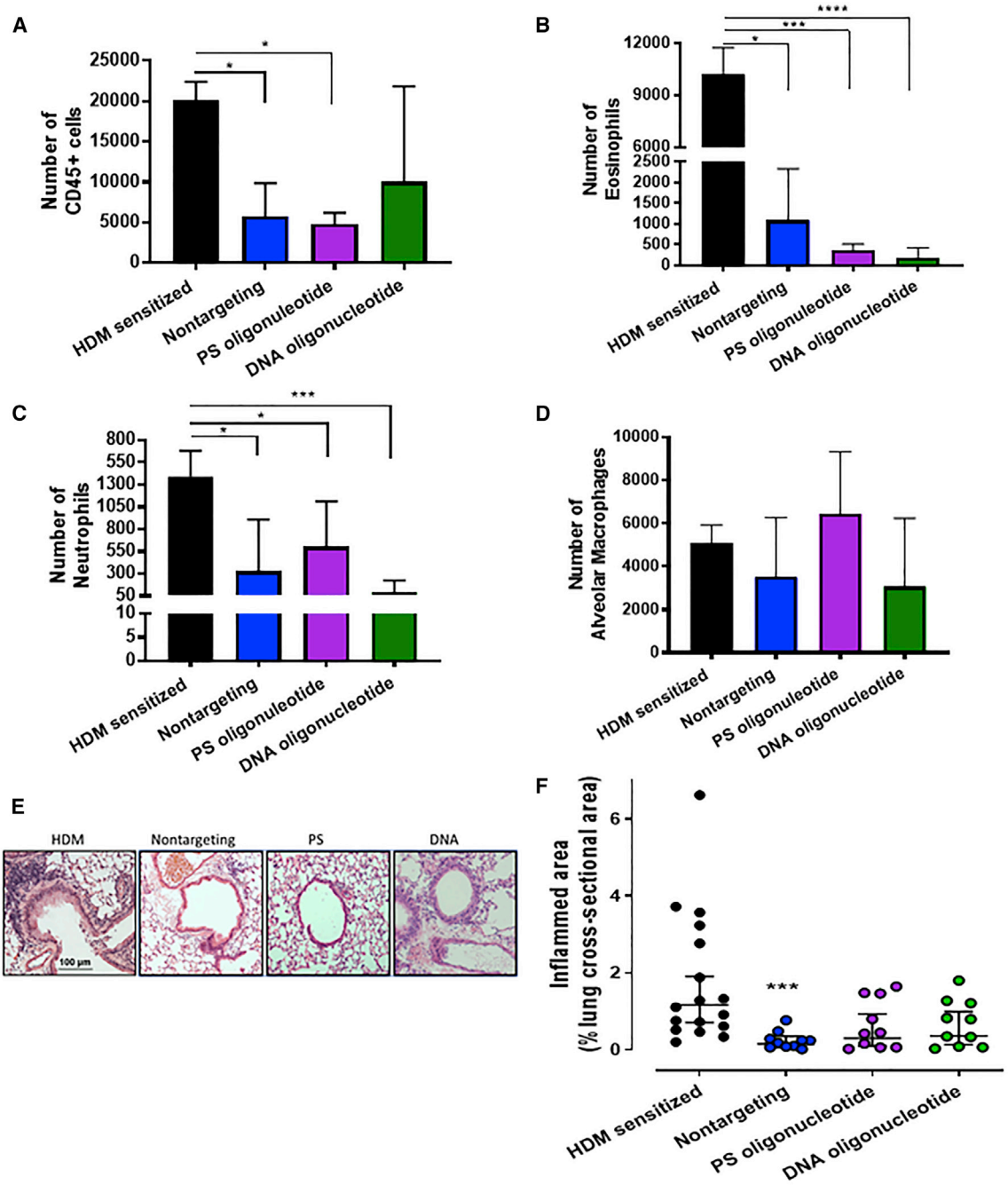

Figure 8. Oligonucleotide Treatment Reduces Immune Cell Infiltration into BALF

(A–D) Differential counts of immune cells in BAL fluid (BALF) were performed by flow cytometry: (A) total CD45+ cells, (B) eosinophils, (C) neutrophils, and (D) alveolar macrophages. Statistical hypothesis testing was performed by Kruskal-Wallis ANOVA and Dunn's post hoc test. *$p < 0.05$; ***$p < 0.005$; ****$p < 0.001$. n = 10–18 mice. (E) Oligonucleotide treatment reduces tissue inflammation. Sections of FFPE lung were stained with H&E to identify sites of inflammation (purple clusters). A representative micrograph for each treatment group is shown. (F) Volume density of inflamed sites was quantified by measuring the area of each site divided by the total cross-sectional area of each lobe. Statistical hypothesis testing was performed with Kruskal-Wallis ANOVA and Dunn's post hoc test using HDM-sensitized mice as the reference group. ***$p < 0.005$. n = 10–17.

formulations of small oligonucleotides with TheraSilence appealing for further development as asthma therapies. We suggest the results provide a rationale for novel oligonucleotide-based polypharmacology approaches to treating Th2 high asthma.

MATERIALS AND METHODS

Oligonucleotides

Two LNA/DNA mixmer oligonucleotides were synthesized with phosphorothioate backbones. The antimiR-145 sequence was 5′-CCTGGGAAAACTGGA-3′ (Exiqon, batch #607391, Woburn, MA, USA). The nontargeting oligonucleotide sequence was 5′-ACGTC TATACGCCCA-3′ (Exiqon, batch #609214). Two additional DNA oligonucleotides were synthesized with the same sequence as that of the nontargeting oligonucleotide, one with a phosphorothioate backbone (PS oligonucleotide) and one with a phosphodiester backbone (DNA oligonucleotide) (Integrated DNA Technology, Coralville, IA, USA).

Liposome Preparation and Formulation

TheraSilence is composed of two lipids, Staramine and Staramine-mPEG, which were synthesized and characterized by Celsion (Huntsville, AL, USA) as described previously.[16,17] To generate TheraSilence cationic liposomes, Staramine and Staramine-mPEG lipids were mixed in chloroform at a 10:1 molar ratio. Following overnight evaporation, the lipid film was rehydrated with water for injection and sonicated in a water bath sonicator for 30 min. Liposomes were further sonicated by a probe sonication using continuous pulse sonication with a 5- to 10-W output (Thermo Fisher Scientific Sonic Dismembrator, Model 100) for 5 min. This procedure typically produced lipid nanoparticles of 80–100 nm in diameter with a zeta potential of 30–50 mV. The liposomes and the oligonucleotides were diluted in 5% dextrose and mixed together in equal volumes to produce a formulation that was 0.2 mg oligonucleotide/mL at a 20:1 N:P ratio (nitrogen:phosphate). The formulation was further concentrated to 0.8 mg/mL using Amicon ultra-centrifugal filter units.

Sensitization with HDM Extract

All studies with mice conformed to guidelines from the U.S. Public Health Service, Office of Laboratory Animal Welfare, for use of animals in research and were approved by the Institutional Animal Care and Use Committee of the University of South Alabama (Mobile, AL, USA). Female BALB/c mice (20–25 g) were anesthetized with 3% isoflurane plus 2 L/min O_2. Milled HDM extract (*Dermatophagoides pteronyssinus,* XPB70D3A2.5, Greer Laboratories, Lenoir, NC, USA) was delivered intranasally (i.n.) as previously described.[15] Mice were sensitized with 50 μL endotoxin-free normal saline containing 50 μg protein on days 0, 1, and 2 (Figure 1A). Unsensitized control mice received 50 μL normal saline and no HDM antigens. Animals were challenged daily with HDM extract (5 μg protein/50 μL, i.n.) on days 14, 15, 16, and 17 to elicit allergic sensitization. Animals were monitored daily for signs of respiratory distress (e.g., dyspnea, hypoxia, lethargy) after allergen sensitization and allergen challenges. No animals required supportive care during this study, which is consistent with the mild/moderate asthma phenotype elicited by short-term HDM exposure. Allergic sensitization was verified by measuring serum levels of total IgG and IgE using commercial ELISA kits (eBiosciences, San Diego, CA, USA). HDM-specific IgG1 and IgE were assayed using a custom ELISA method. Sensitization increased HDM-specific serum IgG and IgE (Figure 1C) but did not significantly increase total IgG1 or IgE as previously described in an acute HDM sensitization model.[25]

ASO Treatments

Oligonucleotides were dissolved in 5% (w/v) dextrose in sterile normal saline solution and then complexed with TheraSilence cationic lipid nanoparticles. Groups of 10 mice were assigned arbitrarily to each treatment group. All mice were injected intravenously (i.v.) via the lateral tail vein on days 13, 15, and 17 with dextrose (placebo control), antimiR-145 (2 mg/kg, i.v.), or nontargeting control oligonucleotides (2 mg/kg, i.v.). Injection volumes never exceeded 5% (w/v) of body mass.

BAL and Flow Cytometry of Immune Cells

BAL was performed by instilling 0.8 mL sterile PBS under 25 cm H_2O pressure and then withdrawing fluid. The process was repeated two more times for a total of 2.4 mL PBS instilled into the lungs with a recovery of 2.1 to 2.3 mL. BAL cells were stained with an antibody cocktail outlined in Table S1. The major innate immune cell populations identified included alveolar macrophages ($CD11c^+$, Siglec F^+), eosinophils ($CD11c^{neg}$, Siglec F^+), and neutrophils ($CD11b^+$, Ly-6G/Gr-1^+). Antibody-labeled cells were washed in 2 mL cold 1× PBS (pH 7.4) and then resuspended in a final volume of 0.3 mL cold PBS prior to flow-cytometric analysis (BD FACSCanto II Flow Cytometer, BD Biosciences, San Jose, CA, USA). Compensation controls from splenocytes were generated using single-antibody-fluorochrome conjugates (shown in Table S2). Cell debris events were excluded by forward scatter × side scatter, and doublet events were excluded by forward scatter height × forward scatter width. All immune cells were gated using CD45. CD45+ cells were then gated with CD11c against Siglec to distinguish alveolar macrophages (CD11c+ Siglec F+), eosinophils ($CD11c^{neg}$ Siglec F^{hi}), and dendritic cells (CD11c+/^{hi} Siglec F^{neg}). The $CD11c^{neg}$ Siglec F^{neg} cells (double-negative gate) were selected and gated with CD11b against Gr-1 to define neutrophils ($CD11b^+$ Gr-1^+). An example of the gating panel is illustrated in Figure S5. Event counts and cell frequencies were calculated to test for differences between treatment groups: unsensitized, HDM sensitized, and sensitized mice treated with oligonucleotides.

Lung Tissue Fixation and Preservation of RNA

After collecting BALF, the thymus and heart were carefully removed. The lobes of the right lung were tied off, removed, and placed in 1 mL RNA*later* RNA Stabilizing Reagent (#76106, QIAGEN, Germantown, MD, USA). The remaining left lung lobe was FFPE and sectioned (5 μm) for histological analysis by H&E staining using standard clinical lab protocols. The RNA*later*-treated lung tissue was placed on ice and then stored at 4°C for a minimum of 24 h prior to long-term storage at −80°C for 2–6 months.

ISH Detection of antimiR-145 and Nontargeting Oligonucleotides

FFPE blocks of mouse lung were cut into sections 5 μm thick, and ISH was used to detect distribution of exogenously administered antimiR-145. Custom DIG-labeled LNA probes (Exiqon) and ISH optimization kits were used according to the manufacturer's instructions (Exiqon, #90-007). The LNA double-DIG-labeled antimir-145 probe was diluted to 60 nM (antimiR-145 and nontargeting oligonucleotides). Anti-DIG alkaline phosphatase (AP) antibody (#11093274910, Sigma-Aldrich, St. Louis, MO, USA) was used to visualize antimiR-145 (Figure 1B). Slides were counterstained with Nuclear Fast Red prior to mounting coverslips.

Tissue CD68+ Immunohistochemistry

CD68+ lung tissue macrophages were assessed by immunohistochemical staining. FFPE lung sections were labeled with anti-CD68 antibody (ab31630, Abcam, Cambridge, MA, USA) and CD68+ cells visualized with Vectastain ABC reagent (PK-6200, Vector Laboratories, Burlingame, CA, USA). All CD68+ cells in an entire lung lobe cross-section were counted in images of 40× fields by an investigator blinded to the treatments. Cells within the alveolar space and erythrocytes in small vessels that were stained brown were excluded from the analysis. The total number of cells per lung section was normalized to the cross-sectional area.

PAS Staining and Mucus Density

Quantitative assessment of mucosal metaplasia was performed by staining FFPE lung slides with PAS stain. Slides were stained according to the manufacturer's instructions (PAS kit #395B-1KT, Sigma, St. Louis, MO, USA) using standard histological techniques. Mucosal metaplasia was quantified from 20× color images that were adjusted to optimize contrast. Mosaic images of airways larger than the field of view were assembled using the Mosaic J Plugin in Fiji (ImageJ v.1, 51j). PAS staining density (points per square millimeter) was measured for every airway in an entire lobe by overlaying a 25 × 25 element grid on 20× images, counting the points intersecting PAS staining, and normalizing points to the total lung cross-sectional area. Point counts were obtained by an operator blinded to the treatment groups. Lung lobe cross-sectional area was measured by scanning PAS-stained slides and a length calibration scale with a Brother MFC 9325CW flatbed scanner calibrated at 1,200 dpi using Adobe Acrobat Pro v.11. TIFF files were imported into Fiji (ImageJ v.1.51) for calculation of the lobe cross-sectional area. Mucus density (points per square millimeter) was further stratified by airway diameter (<100 μm, 100–300 μm, 300–600 μm, and >600 μm).

Sirius Red Staining and Eosinophil Counts

Eosinophil infiltration into lung tissue was measured by staining FFPE sections with Sirius red.[53] Total lung lobe cross-sectional area was measured by scanning slides with a flatbed scanner calibrated at 1,200 dpi using Adobe Acrobat Pro v.11. The area of each lung lobe analyzed was calculated using Fiji (ImageJ v.1.51n). All eosinophils in a given lung section were counted by collecting 40× images of the entire lung section by an investigator blinded to the treatments. Eosinophils adjacent to blood vessels and airways were identified by purple bilobular nuclei and bright pink cytoplasm. Cells with lighter and translucent cytoplasm were excluded from the analysis. The total number of cells in a lung section was normalized to the cross-sectional area to estimate volume density of lung tissue eosinophils.

Western Blotting

Protein samples were prepared by extracting total SDS-soluble proteins in a buffer containing 60 mM Tris-HCl (pH 6.8), 2% SDS, 10% glycerol, 1 mM K_2EGTA, 1 mM Na_2EDTA, 5 mM NaF, and 1× Mini cOmplete protease inhibitor (Sigma-Aldrich, St. Louis, MO, USA). Right lung lobes were minced into 2- to 3-mm pieces and then homogenized immediately using BioSpec glass beads (11079110, Bartlesville, OK, USA) and a Mini-Bead Beater-16. Protein concentrations of clarified homogenates (12,000 × *g*, 10 min, 4°C) were determined using the bicinchoninic acid assay.[54] Proteins were resolved by SDS-PAGE and transferred to nitrocellulose. Equal loading was verified using BLOT-FastStain (G-Biosciences, St. Louis, MO, USA). Primary antibodies and dilutions used in immunoblotting were: alpha-actin (A2547, Sigma-Aldrich; 1:2,000), SM22 (Ab14106, Abcam; 1:5,000), MHC (MA: BT-562, Alfa Aesar, Haverhill, MA, USA; 1:2,000), and KLF4 (4038S, Cell Signaling Technology, Danvers, MA, USA; 1:100). Fluorescent secondary antibodies (IRDye 680LT and 800CW, 1:20,000) were detected with an Odyssey near-infrared laser scanner (LI-COR, Lincoln, NE, USA). Sample loading and antibody dilutions were optimized in preliminary studies to be within the linear range of signal intensity. Integrated intensities were corrected for differences in total protein staining. Contractile protein immunoreactivity was normalized to the immunoreactivity of human tracheal smooth muscle proteins (5 μg protein) loaded on the same gel and western blot.

RNA Isolation and qRT-PCR

Lung lobes stored for 2–6 months in RNA*later* solution were weighed (~25–30 mg) and minced into 2- to 3-mm pieces. Total RNA was extracted with QIAzol Lysis Reagent (1023537, QIAGEN, Germantown, MD, USA) using zirconia beads (BioSpec, 11079110ZX) and a Mini-Bead Beater-16. Total RNA, including miRNA, was isolated using a QIAGEN miRNEasy Kit (#217004) following the manufacturer's protocol including treatment with DNAase. Yield ranged from 15 to 33 μg total RNA per lung lobe, with the higher yields from lungs of allergic sensitized mice. Three methods were used to determine RNA concentration and RNA quality: spectrophotometry of total RNA (NanoDrop 1000), gel filtration of RNA integrity (RNA 6000 Nano Kit, Agilent 2100 Bioanalyzer), and fluorescent dye binding (Quant-iT RiboGreen Kit,[55] Invitrogen, Carlsbad, CA, USA). RNA quality determined by A260/280 ranged from 1.8 to 2.2, A260/230 > 2, and RNA integrity (RIN) values ranged from 6.9 to 8.6.

qRT-PCR was used to quantify relative expression levels of mRNAs in lung tissue. Total RNA (10 ng) was reverse transcribed to cDNA using an iScript cDNA Synthesis Kit (170-8891, Bio-Rad, Hercules, CA, USA) according to the manufacturer's instructions. cDNA was stored at −80°C until used in real-time PCR assays. SYBR Green I real-time

PCR assays were performed using 2 μL cDNA in a reaction volume of 20 μL in a CFX96 thermocycler (Bio-Rad). Amplicons were detected using iQ SYBR Green Supermix reagents (Bio-Rad, 1708882) with 300 nM of each forward and reverse primer. Forward and reverse primers manufactured by Integrated DNA Technology (Coralville, IA, USA) are listed in Table S3. Several mouse transcripts commonly used as reference controls (*Eif2*, *B2m*, and *Hprt*)[56] were tested under the various treatments used in the study. *Hprt* was the only transcript of this group unaffected by the various treatments. Therefore, target mRNA expression was calculated relative to *Hprt* (Ensembl:ENSMUSG00000025630) using established ΔΔCq methods. PCR data were analyzed using CFX Manager software to adjust thresholds and calculate Cq for each reaction. Primer specificity was assessed *in silico* and by conducting melt curves of amplicons following PCR. DNA contamination was eliminated by DNase treatment during preparation of total RNA. DNA contamination of cDNA was assessed using exon-spanning primers for the *Hprt* reference gene and by including no template-negative controls in all studies.

Quantitative real-time PCR for miRNA was used to quantify the expression of native mature mmu-miR-145a-5p (miRbase:MIMAT0000157) using TaqMan detection kits. Total RNA (1–10 ng) was reverse transcribed into cDNA using the TaqMan MicroRNA Reverse Transcription Kit according to the manufacturer's instructions (#4366596, Applied Biosystems, Foster City, CA, USA). miRNA standard curves (0.001 to 100 pg) were generated using a synthetic miR-145-5p 22-nt RNA oligonucleotide (guccaguuuucccaggaaucc) manufactured by Integrated DNA Technologies (Coralville, IA, USA); r2 > 0.9 and slopes > 3.0.

Poly(A) RNA-Seq

Total RNA from a single lung lobe underwent quality control checks using an Agilent 2100 Bioanalyzer prior to library construction. RIN for all samples ranged from 6.9 to 8.6. Libraries were then constructed from poly(A)-selected RNA by the Genomic Services Lab at the Hudson Alpha Institute of Biotechnology (Huntsville, AL, USA). Initial RNA quantification was performed with a Qubit RNA Assay Kit, followed by RIN determination with an Agilent 2100 Bioanalyzer and final quantification with a KAPA Library Quantification Kit. Nonstranded libraries were sequenced at 15.6 million reads per sample for the HDM and antimiR-145 groups and 10 million reads per sample for the unsensitized and nontargeting-oligonucleotide groups. 100-nt, paired-end sequences were generated using an Illumina HiSeq2500 sequencer.

Bioinformatics Methods

Fastqsanger sequence files were analyzed using the Globus Genomics cloud-based implementation of the Galaxy interface for next generation sequence data analysis (https://globusgenomics.org).[57,58] The analysis pipeline included FastQC, Trimmomatic,[59] STAR,[60] featureCounts,[61] and DESeq2.[62] All quality scores of trimmed sequence data were >30. DESeq2 was used to generate differential expression data comparing $\log_2$ fold change between treatment groups. The sign of the $\log_2$ fold change and p value from the Wald test was used to calculate an enrichment score (ES) for each transcript: ES = sign ($\log_2$ fold change) · 1/p value.[63] The data were then filtered to remove genes with a false discovery rate (FDR) > 0.2. Genes ranked by ES were used as input into GSEA.[64] An FDR threshold of 0.2 was selected because the low number of genes in most sets being analyzed would increase the chances of overlooking biologically important results if the FDR were more stringent.[64] Differences in expression of the gene set are illustrated by dot plots of the rank versus ES of each transcript in the set (see Figure 5). Upward deflection of the trend line above 0 indicates enrichment of transcripts that were upregulated. Gene sets were built from the literature on human asthma,[23,24] mouse models of asthma,[25] and mucin production[50] and microarray studies of the biology of inflammation and development published in MSigDB collections.[65–75] Significant changes in gene sets associated with each treatment were visualized by plotting a normalized ES (NES) for each gene set versus the pathway (Figure 6). The genes in each reference set are listed in Table S5.

Statistical Analyses

Statistical analysis of RNA-seq data was conducted as described by Love et al.[62] for DESeq2 differential expression. NESs generated by GSEA were calculated as described by Subramanian et al.[64] and the GSEA documentation (http://software.broadinstitute.org/gsea). Statistical analyses of protein expression, morphometric studies, and RT-PCR were performed using GraphPad Prism (v.7, San Diego, CA, USA). Prospective power analysis was performed to estimate that 10 biological replicates were needed to detect a 40% true difference between means if $\sigma = 0.3$. The calculation was based on a two-sample t test model, $\alpha = 0.05$, $p < 0.05$, power = 0.81. Selected pairs of treatments were compared using one-way ANOVA with Bonferroni's test for data that were normally distributed. When each treatment was compared to a defined reference group (HDM sensitized), one-way ANOVA and Dunnett's test were used for normally distributed data. When datasets failed the D'Agostino-Pearson test of normality, non-parametric ANOVA was performed with Dunn's post hoc test. Dunnett's and Dunn's post hoc tests were performed using HDM-sensitized animals as the reference group. The null hypothesis was that any other treatment was not different from HDM-sensitized, dextrose-treated animals.

SUPPLEMENTAL INFORMATION

Supplemental Information can be found online at https://doi.org/10.1016/j.omtn.2019.12.033.

AUTHOR CONTRIBUTIONS

Conceptualization: W.T.G., S.C.R., and R.B.; Methodology: W.T.G., S.C.R., B.S.C., J.M.M., L.L.S., and A.P.F.; Investigation: W.T.G., S.C.R., L.L.S., and A.P.F.; Formal Analysis: W.T.G., S.C.R., and J.M.M.; Resources: R.B., J.S., M.M., and J.F.; Writing – Original Draft: W.T.G. and S.C.R.; Writing – Review & Editing: B.S.C., J.M.M., R.B., and J.S.; Funding Acquisition: W.T.G. and R.B.; Supervision: W.T.G. and R.B.

ACKNOWLEDGMENTS

We thank Jessica Bell, Ileana Aragon, Jacqueria Tucker, William Browning, and Ning Cheng for technical assistance. This research was supported by NIH grants HL077726, UL1TR001417, and AI116985 (to W.T.G. and R.B.). This publication was made possible by an NIH grant from the National Institute of General Medical Sciences (GM103440). Research support was also provided by the Office of Medical Research, University of Nevada, Reno. TheraSilence formulations were provided by Celsion (Huntsville, AL, USA).

REFERENCES

1. Gross, N.J., and Barnes, P.J. (2017). New therapies for asthma and chronic obstructive pulmonary disease. Am. J. Respir. Crit. Care Med. *195*, 159–166.
2. Kuruvilla, M.E., Lee, F.E., and Lee, G.B. (2019). Understanding asthma phenotypes, endotypes, and mechanisms of disease. Clin. Rev. Allergy Immunol. *56*, 219–233.
3. Pelaia, G., Canonica, G.W., Matucci, A., Paolini, R., Triggiani, M., and Paggiaro, P. (2017). Targeted therapy in severe asthma today: focus on immunoglobulin E. Drug Des. Devel. Ther. *11*, 1979–1987.
4. Pua, H.H., and Ansel, K.M. (2015). MicroRNA regulation of allergic inflammation and asthma. Curr. Opin. Immunol. *36*, 101–108.
5. Comer, B.S., Ba, M., Singer, C.A., and Gerthoffer, W.T. (2015). Epigenetic targets for novel therapies of lung diseases. Pharmacol. Ther. *147*, 91–110.
6. Brook, P.O., Perry, M.M., Adcock, I.M., and Durham, A.L. (2015). Epigenome-modifying tools in asthma. Epigenomics *7*, 1017–1032.
7. van den Berge, M., and Tasena, H. (2019). Role of microRNAs and exosomes in asthma. Curr. Opin. Pulm. Med. *25*, 87–93.
8. Molfino, N.A., Gossage, D., Kolbeck, R., Parker, J.M., and Geba, G.P. (2012). Molecular and clinical rationale for therapeutic targeting of interleukin-5 and its receptor. Clin. Exp. Allergy *42*, 712–737.
9. Luo, Y., Pang, Z., Zhu, Q., Cai, X., Yin, Y., Wang, M., Zhu, J., Chen, J., Zeng, K., Zhang, C., and Zhang, J. (2012). Locally instilled tumor necrosis factor-α antisense oligonucleotide inhibits allergic inflammation via the induction of Tregs. J. Gene Med. *14*, 374–383.
10. Tian, X.R., Tian, X.L., Bo, J.P., Li, S.G., Liu, Z.L., and Niu, B. (2011). Inhibition of allergic airway inflammation by antisense-induced blockade of STAT6 expression. Chin. Med. J. (Engl.) *124*, 26–31.
11. Duan, W., Chan, J.H., McKay, K., Crosby, J.R., Choo, H.H., Leung, B.P., Karras, J.G., and Wong, W.S. (2005). Inhaled p38alpha mitogen-activated protein kinase antisense oligonucleotide attenuates asthma in mice. Am. J. Respir. Crit. Care Med. *171*, 571–578.
12. Pagdin, T., and Lavender, P. (2012). MicroRNAs in lung diseases. Thorax *67*, 183–184.
13. Foster, P.S., Plank, M., Collison, A., Tay, H.L., Kaiko, G.E., Li, J., Johnston, S.L., Hansbro, P.M., Kumar, R.K., Yang, M., and Mattes, J. (2013). The emerging role of microRNAs in regulating immune and inflammatory responses in the lung. Immunol. Rev. *253*, 198–215.
14. Fekonja, S., Korošec, P., Rijavec, M., Jeseničnik, T., and Kunej, T. (2018). Asthma microRNA regulome development using validated miRNA-target interaction visualization. OMICS *22*, 607–615.
15. Collison, A., Mattes, J., Plank, M., and Foster, P.S. (2011). Inhibition of house dust mite-induced allergic airways disease by antagonism of microRNA-145 is comparable to glucocorticoid treatment. J. Allergy Clin. Immunol. *128*, 160–167.e4.
16. Sparks, J., Slobodkin, G., Matar, M., Congo, R., Ulkoski, D., Rea-Ramsey, A., Pence, C., Rice, J., McClure, D., Polach, K.J., et al. (2012). Versatile cationic lipids for siRNA delivery. J. Control. Release *158*, 269–276.
17. Polach, K.J., Matar, M., Rice, J., Slobodkin, G., Sparks, J., Congo, R., Rea-Ramsey, A., McClure, D., Brunhoeber, E., Krampert, M., et al. (2012). Delivery of siRNA to the mouse lung via a functionalized lipopolyamine. Mol. Ther. *20*, 91–100.
18. McLendon, J.M., Joshi, S.R., Sparks, J., Matar, M., Fewell, J.G., Abe, K., Oka, M., McMurtry, I.F., and Gerthoffer, W.T. (2015). Lipid nanoparticle delivery of a microRNA-145 inhibitor improves experimental pulmonary hypertension. J. Control. Release *210*, 67–75.
19. Ramelli, S., McLendon, J.M., Ferretti, A.P., Fewell, J., Barrington, R., and Gerthoffer, W.T. (2016). Antisense microRNA therapy of airway remodeling in house dust mite-sensitized mice. Ann. Am. Thorac. Soc. *13* (*Suppl 1*), S101–S102.
20. Evans, C.M., Williams, O.W., Tuvim, M.J., Nigam, R., Mixides, G.P., Blackburn, M.R., DeMayo, F.J., Burns, A.R., Smith, C., Reynolds, S.D., et al. (2004). Mucin is produced by clara cells in the proximal airways of antigen-challenged mice. Am. J. Respir. Cell Mol. Biol. *31*, 382–394.
21. Evans, C.M., Raclawska, D.S., Ttofali, F., Liptzin, D.R., Fletcher, A.A., Harper, D.N., McGing, M.A., McElwee, M.M., Williams, O.W., Sanchez, E., et al. (2015). The polymeric mucin Muc5ac is required for allergic airway hyperreactivity. Nat. Commun. *6*, 6281.
22. Maragkakis, M., Vergoulis, T., Alexiou, P., Reczko, M., Plomaritou, K., Gousis, M., Kourtis, K., Koziris, N., Dalamagas, T., and Hatzigeorgiou, A.G. (2011). DIANA-microT Web server upgrade supports Fly and Worm miRNA target prediction and bibliographic miRNA to disease association. Nucleic Acids Res. *39*, W145–W148.
23. Woodruff, P.G., Boushey, H.A., Dolganov, G.M., Barker, C.S., Yang, Y.H., Donnelly, S., Ellwanger, A., Sidhu, S.S., Dao-Pick, T.P., Pantoja, C., et al. (2007). Genome-wide profiling identifies epithelial cell genes associated with asthma and with treatment response to corticosteroids. Proc. Natl. Acad. Sci. USA *104*, 15858–15863.
24. Choy, D.F., Hart, K.M., Borthwick, L.A., Shikotra, A., Nagarkar, D.R., Siddiqui, S., Jia, G., Ohri, C.M., Doran, E., Vannella, K.M., et al. (2015). TH2 and TH17 inflammatory pathways are reciprocally regulated in asthma. Sci. Transl. Med. *7*, 301ra129.
25. Piyadasa, H., Altieri, A., Basu, S., Schwartz, J., Halayko, A.J., and Mookherjee, N. (2016). Biosignature for airway inflammation in a house dust mite-challenged murine model of allergic asthma. Biol. Open *5*, 112–121.
26. Woodruff, P.G., Modrek, B., Choy, D.F., Jia, G., Abbas, A.R., Ellwanger, A., Koth, L.L., Arron, J.R., and Fahy, J.V. (2009). T-helper type 2-driven inflammation defines major subphenotypes of asthma. Am. J. Respir. Crit. Care Med. *180*, 388–395.
27. Jevnikar, Z., Östling, J., Ax, E., Calvén, J., Thorn, K., Israelsson, E., Öberg, L., Singhania, A., Lau, L.C.K., Wilson, S.J., et al. (2019). Epithelial IL-6 trans-signaling defines a new asthma phenotype with increased airway inflammation. J. Allergy Clin. Immunol. *143*, 577–590.
28. Phuc Le, P., Friedman, J.R., Schug, J., Brestelli, J.E., Parker, J.B., Bochkis, I.M., and Kaestner, K.H. (2005). Glucocorticoid receptor-dependent gene regulatory networks. PLoS Genet. *1*, e16.
29. Vukmirovic, M., Herazo-Maya, J.D., Blackmon, J., Skodric-Trifunovic, V., Jovanovic, D., Pavlovic, S., Stojsic, J., Zeljkovic, V., Yan, X., Homer, R., et al. (2017). Identification and validation of differentially expressed transcripts by RNA-sequencing of formalin-fixed, paraffin-embedded (FFPE) lung tissue from patients with idiopathic pulmonary fibrosis. BMC Pulm. Med. *17*, 15.
30. Miano, J.M. (2003). Serum response factor: toggling between disparate programs of gene expression. J. Mol. Cell. Cardiol. *35*, 577–593.
31. Nelander, S., Mostad, P., and Lindahl, P. (2003). Prediction of cell type-specific gene modules: identification and initial characterization of a core set of smooth muscle-specific genes. Genome Res. *13*, 1838–1854.
32. Larsson, E., McLean, S.E., Mecham, R.P., Lindahl, P., and Nelander, S. (2008). Do two mutually exclusive gene modules define the phenotypic diversity of mammalian smooth muscle? Mol. Genet. Genomics *280*, 127–137.
33. Wark, P.A., Johnston, S.L., Bucchieri, F., Powell, R., Puddicombe, S., Laza-Stanca, V., Holgate, S.T., and Davies, D.E. (2005). Asthmatic bronchial epithelial cells have a deficient innate immune response to infection with rhinovirus. J. Exp. Med. *201*, 937–947.
34. Sarvestani, S.T., Stunden, H.J., Behlke, M.A., Forster, S.C., McCoy, C.E., Tate, M.D., Ferrand, J., Lennox, K.A., Latz, E., Williams, B.R., and Gantier, M.P. (2015). Sequence-dependent off-target inhibition of TLR7/8 sensing by synthetic microRNA inhibitors. Nucleic Acids Res. *43*, 1177–1188.
35. Look, M., Saltzman, W.M., Craft, J., and Fahmy, T.M. (2014). The nanomaterial-dependent modulation of dendritic cells and its potential influence on therapeutic immunosuppression in lupus. Biomaterials *35*, 1089–1095.
36. Wenzel, S. (2003). Severe/fatal asthma. Chest *123* (3, Suppl), 405S–410S.

37. Barnes, P.J. (2004). Corticosteroid resistance in airway disease. Proc. Am. Thorac. Soc. *1*, 264–268.

38. Trevor, J.L., and Deshane, J.S. (2014). Refractory asthma: mechanisms, targets, and therapy. Allergy *69*, 817–827.

39. Fahy, J.V. (2015). Type 2 inflammation in asthma–present in most, absent in many. Nat. Rev. Immunol. *15*, 57–65.

40. Gauthier, M., Ray, A., and Wenzel, S.E. (2015). Evolving concepts of asthma. Am. J. Respir. Crit. Care Med. *192*, 660–668.

41. Robinson, D.S., Kariyawasam, H.H., and Heaney, L.G. (2017). Phase three studies of biologics for severe asthma: could do better? Eur. Respir. J. *50*, 1701108.

42. Garbacki, N., Di Valentin, E., Huynh-Thu, V.A., Geurts, P., Irrthum, A., Crahay, C., Arnould, T., Deroanne, C., Piette, J., Cataldo, D., and Colige, A. (2011). MicroRNAs profiling in murine models of acute and chronic asthma: a relationship with mRNAs targets. PLoS ONE *6*, e16509.

43. Collison, A., Siegle, J.S., Hansbro, N.G., Kwok, C.T., Herbert, C., Mattes, J., Hitchins, M., Foster, P.S., and Kumar, R.K. (2013). Epigenetic changes associated with disease progression in a mouse model of childhood allergic asthma. Dis. Model. Mech. *6*, 993–1000.

44. Ameis, D., Khoshgoo, N., Iwasiow, B.M., Snarr, P., and Keijzer, R. (2017). MicroRNAs in lung development and disease. Paediatr. Respir. Rev. *22*, 38–43.

45. Williams, A.E., Larner-Svensson, H., Perry, M.M., Campbell, G.A., Herrick, S.E., Adcock, I.M., Erjefalt, J.S., Chung, K.F., and Lindsay, M.A. (2009). MicroRNA expression profiling in mild asthmatic human airways and effect of corticosteroid therapy. PLoS ONE *4*, e5889.

46. Cordes, K.R., Sheehy, N.T., White, M.P., Berry, E.C., Morton, S.U., Muth, A.N., Lee, T.H., Miano, J.M., Ivey, K.N., and Srivastava, D. (2009). miR-145 and miR-143 regulate smooth muscle cell fate and plasticity. Nature *460*, 705–710.

47. Liu, Y., Sun, X., Wu, Y., Fang, P., Shi, H., Xu, J., and Li, M. (2015). Effects of miRNA-145 on airway smooth muscle cells function. Mol. Cell. Biochem. *409*, 135–143.

48. Yang, S., Cui, H., Xie, N., Icyuz, M., Banerjee, S., Antony, V.B., Abraham, E., Thannickal, V.J., and Liu, G. (2013). miR-145 regulates myofibroblast differentiation and lung fibrosis. FASEB J. *27*, 2382–2391.

49. O'Leary, L., Sevinç, K., Papazoglou, I.M., Tildy, B., Detillieux, K., Halayko, A.J., Chung, K.F., and Perry, M.M. (2016). Airway smooth muscle inflammation is regulated by microRNA-145 in COPD. FEBS Lett. *590*, 1324–1334.

50. Wang, G., Xu, Z., Wang, R., Al-Hijji, M., Salit, J., Strulovici-Barel, Y., Tilley, A.E., Mezey, J.G., and Crystal, R.G. (2012). Genes associated with MUC5AC expression in small airway epithelium of human smokers and non-smokers. BMC Med. Genomics *5*, 21.

51. Contoli, M., Message, S.D., Laza-Stanca, V., Edwards, M.R., Wark, P.A., Bartlett, N.W., Kebadze, T., Mallia, P., Stanciu, L.A., Parker, H.L., et al. (2006). Role of deficient type III interferon-lambda production in asthma exacerbations. Nat. Med. *12*, 1023–1026.

52. Gavala, M.L., Bashir, H., and Gern, J.E. (2013). Virus/allergen interactions in asthma. Curr. Allergy Asthma Rep. *13*, 298–307.

53. Meyerholz, D.K., Griffin, M.A., Castilow, E.M., and Varga, S.M. (2009). Comparison of histochemical methods for murine eosinophil detection in an RSV vaccine-enhanced inflammation model. Toxicol. Pathol. *37*, 249–255.

54. Smith, P.K., Krohn, R.I., Hermanson, G.T., Mallia, A.K., Gartner, F.H., Provenzano, M.D., Fujimoto, E.K., Goeke, N.M., Olson, B.J., and Klenk, D.C. (1985). Measurement of protein using bicinchoninic acid. Anal. Biochem. *150*, 76–85.

55. Aranda, R., 4th, Dineen, S.M., Craig, R.L., Guerrieri, R.A., and Robertson, J.M. (2009). Comparison and evaluation of RNA quantification methods using viral, prokaryotic, and eukaryotic RNA over a 10(4) concentration range. Anal. Biochem. *387*, 122–127.

56. Lee, D.D., and Schwarz, M.A. (2015). Adapted approach to profile genes while reconciling Vegf-a mRNA expression in the developing and injured lung. Am. J. Physiol. Lung Cell. Mol. Physiol. *308*, L1202–L1211.

57. Madduri, R.K., Sulakhe, D., Lacinski, L., Liu, B., Rodriguez, A., Chard, K., Dave, U.J., and Foster, I.T. (2014). Experiences building Globus Genomics: a next-generation sequencing analysis service using Galaxy, Globus, and Amazon web services. Concurr. Comput. *26*, 2266–2279.

58. Afgan, E., Baker, D., Batut, B., van den Beek, M., Bouvier, D., Cech, M., Chilton, J., Clements, D., Coraor, N., Grüning, B.A., et al. (2018). The Galaxy platform for accessible, reproducible and collaborative biomedical analyses: 2018 update. Nucleic Acids Res. *46* (W1), W537–W544.

59. Bolger, A.M., Lohse, M., and Usadel, B. (2014). Trimmomatic: a flexible trimmer for Illumina sequence data. Bioinformatics *30*, 2114–2120.

60. Dobin, A., and Gingeras, T.R. (2016). Optimizing RNA-seq mapping with STAR. Methods Mol. Biol. *1415*, 245–262.

61. Liao, Y., Smyth, G.K., and Shi, W. (2014). featureCounts: an efficient general purpose program for assigning sequence reads to genomic features. Bioinformatics *30*, 923–930.

62. Love, M.I., Huber, W., and Anders, S. (2014). Moderated estimation of fold change and dispersion for RNA-seq data with DESeq2. Genome Biol. *15*, 550.

63. Plaisier, S.B., Taschereau, R., Wong, J.A., and Graeber, T.G. (2010). Rank-rank hypergeometric overlap: identification of statistically significant overlap between gene-expression signatures. Nucleic Acids Res. *38*, e169.

64. Subramanian, A., Tamayo, P., Mootha, V.K., Mukherjee, S., Ebert, B.L., Gillette, M.A., Paulovich, A., Pomeroy, S.L., Golub, T.R., Lander, E.S., and Mesirov, J.P. (2005). Gene set enrichment analysis: a knowledge-based approach for interpreting genome-wide expression profiles. Proc. Natl. Acad. Sci. USA *102*, 15545–15550.

65. Liberzon, A., Birger, C., Thorvaldsdóttir, H., Ghandi, M., Mesirov, J.P., and Tamayo, P. (2015). The Molecular Signatures Database (MSigDB) hallmark gene set collection. Cell Syst. *1*, 417–425.

66. Quintavalle, M., Elia, L., Condorelli, G., and Courtneidge, S.A. (2010). MicroRNA control of podosome formation in vascular smooth muscle cells in vivo and in vitro. J. Cell Biol. *189*, 13–22.

67. Chiyomaru, T., Enokida, H., Tatarano, S., Kawahara, K., Uchida, Y., Nishiyama, K., Fujimura, L., Kikkawa, N., Seki, N., and Nakagawa, M. (2010). miR-145 and miR-133a function as tumour suppressors and directly regulate FSCN1 expression in bladder cancer. Br. J. Cancer *102*, 883–891.

68. Schmitt, M.M., Megens, R.T., Zernecke, A., Bidzhekov, K., van den Akker, N.M., Rademakers, T., van Zandvoort, M.A., Hackeng, T.M., Koenen, R.R., and Weber, C. (2014). Endothelial junctional adhesion molecule-a guides monocytes into flow-dependent predilection sites of atherosclerosis. Circulation *129*, 66–76.

69. Oglesby, I.K., Chotirmall, S.H., McElvaney, N.G., and Greene, C.M. (2013). Regulation of cystic fibrosis transmembrane conductance regulator by microRNA-145, -223, and -494 is altered in ΔF508 cystic fibrosis airway epithelium. J. Immunol. *190*, 3354–3362.

70. Viart, V., Bergougnoux, A., Bonini, J., Varilh, J., Chiron, R., Tabary, O., Molinari, N., Claustres, M., and Taulan-Cadars, M. (2015). Transcription factors and miRNAs that regulate fetal to adult CFTR expression change are new targets for cystic fibrosis. Eur. Respir. J. *45*, 116–128.

71. Booiman, T., Cobos Jiménez, V., van Dort, K.A., van 't Wout, A.B., and Kootstra, N.A. (2014). Phosphodiesterase 8a supports HIV-1 replication in macrophages at the level of reverse transcription. PLoS ONE *9*, e109673.

72. Zhou, J., Chaudhry, H., Zhong, Y., Ali, M.M., Perkins, L.A., Owens, W.B., Morales, J.E., McGuire, F.R., Zumbrun, E.E., Zhang, J., et al. (2015). Dysregulation in microRNA expression in peripheral blood mononuclear cells of sepsis patients is associated with immunopathology. Cytokine *71*, 89–100.

73. Fayyad-Kazan, H., Rouas, R., Fayyad-Kazan, M., Badran, R., El Zein, N., Lewalle, P., Najar, M., Hamade, E., Jebbawi, F., Merimi, M., et al. (2012). MicroRNA profile of circulating CD4-positive regulatory T cells in human adults and impact of differentially expressed microRNAs on expression of two genes essential to their function. J. Biol. Chem. *287*, 9910–9922.

74. Xu, N., Papagiannakopoulos, T., Pan, G., Thomson, J.A., and Kosik, K.S. (2009). MicroRNA-145 regulates OCT4, SOX2, and KLF4 and represses pluripotency in human embryonic stem cells. Cell *137*, 647–658.

75. Mayorga, M.E., and Penn, M.S. (2012). miR-145 is differentially regulated by TGF-β1 and ischaemia and targets Disabled-2 expression and wnt/β-catenin activity. J. Cell. Mol. Med. *16*, 1106–1113.

OMTN, Volume *19*

Supplemental Information

Nanoparticle Delivery of Anti-inflammatory LNA Oligonucleotides Prevents Airway Inflammation in a HDM Model of Asthma

Sabrina C. Ramelli, Brian S. Comer, Jared M. McLendon, Lydia L. Sandy, Andrew P. Ferretti, Robert Barrington, Jeff Sparks, Majed Matar, Jason Fewell, and William T. Gerthoffer

Supplemental Data

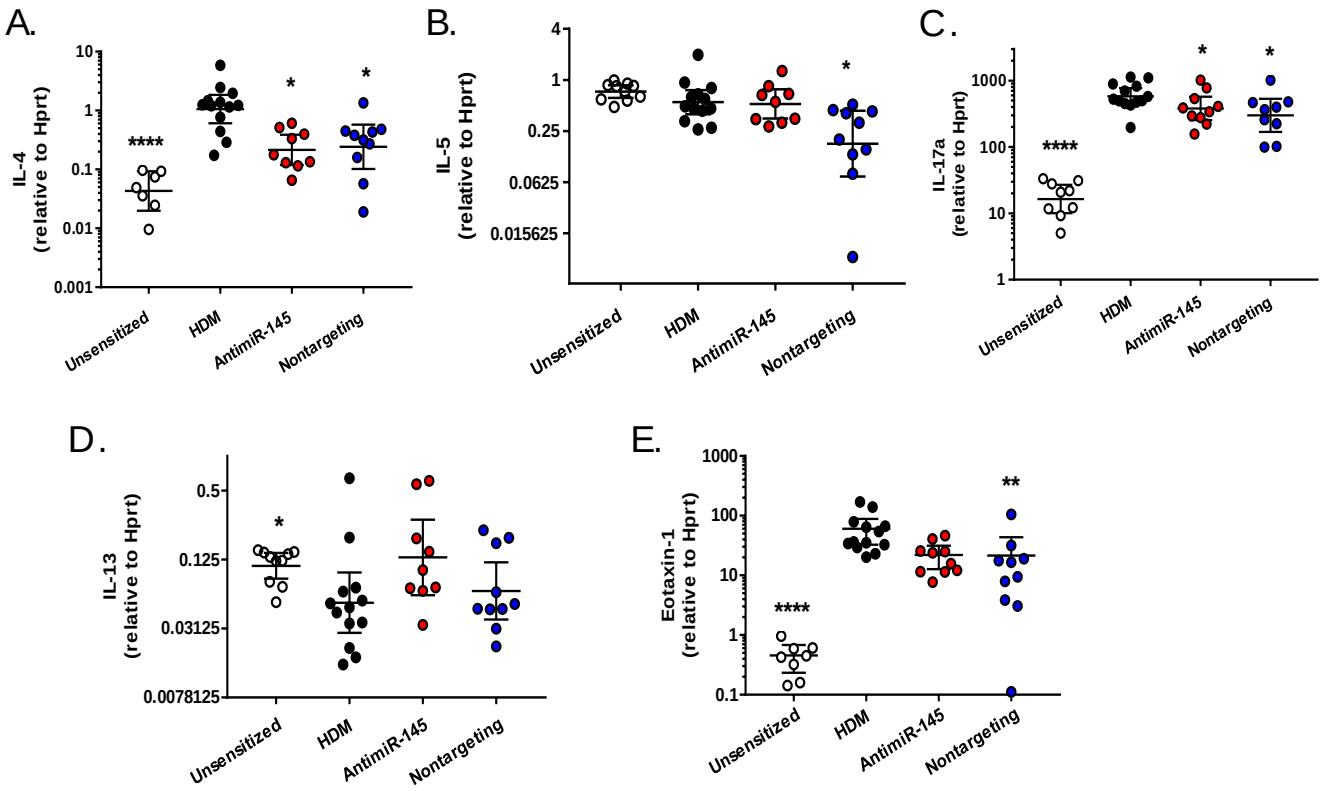

Figure S1. AntimiR-145 reduces expression of IL-4. qRT-PCR of isolated RNA of mouse lungs to determine the differences between treatment groups of (A) IL-4, (B) IL-5, (C) IL-13, (D) IL-17a, and (E) Eotaxin-1. Data are shown as means and 95% confidence intervals. Statistical analyses was performed by Kruskal-Wallis ANOVA with Dunn's post hoc test, * $p \leq 0.05$, *** $p \leq 0.01$, n = 9-13.

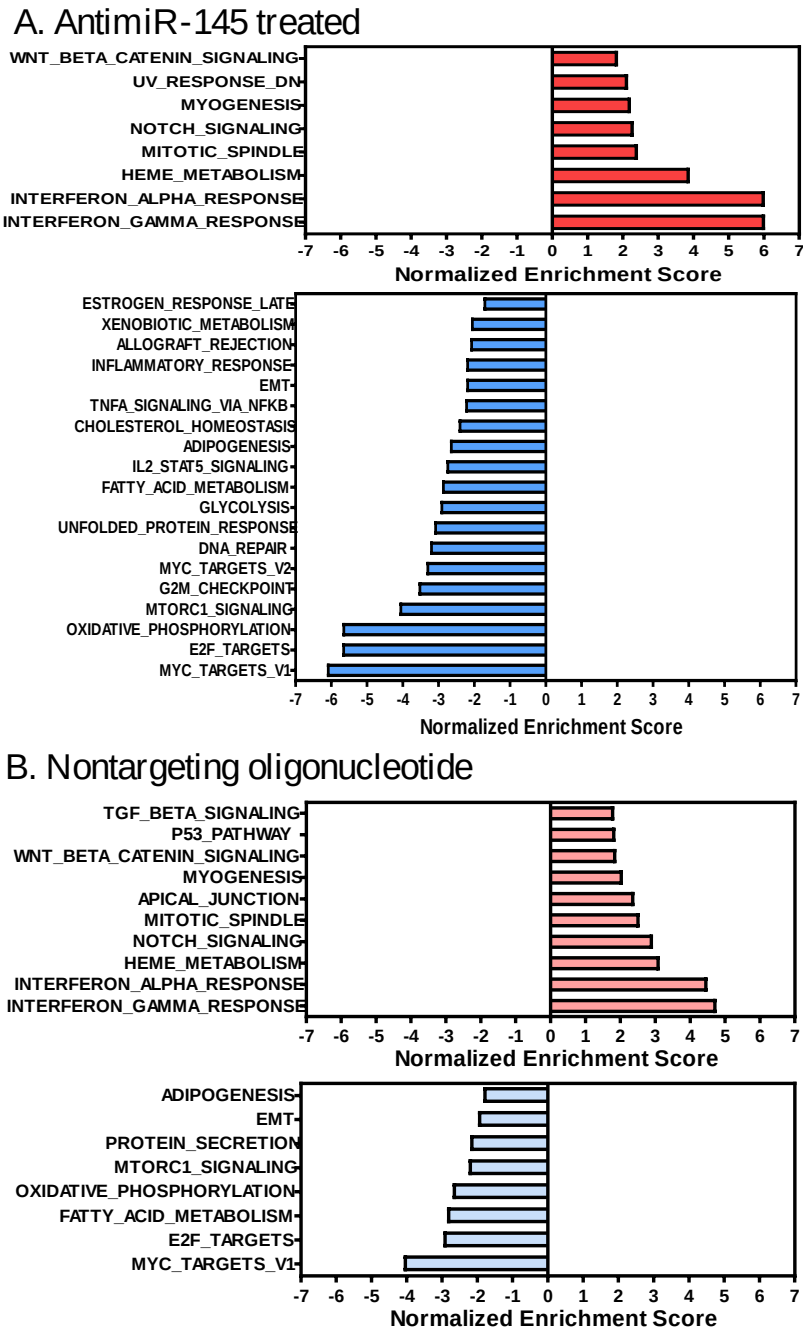

Figure S2. HDM-enhanced expression of Hallmark pathways is differentially affected by antimiR-145 compared to nontargeting oligonucleotide. Gene set enrichment analysis (GSEA) was performed using whole lung poly A RNA-seq data from HDM-sensitized mice treated with dextrose as the reference group. (A) Changes in signaling and metabolic pathways genes in the Hallmarks gene set of the MSigDB collection in HDM-sensitized mice treated with antimiR-145 (2 mg/kg, iv); FDR < 0.05. (B) Changes in signaling and metabolic pathways genes in HDM-sensitized mice treated with nontargeting oligonucleotide (2 mg/kg, iv); FDR < 0.05.

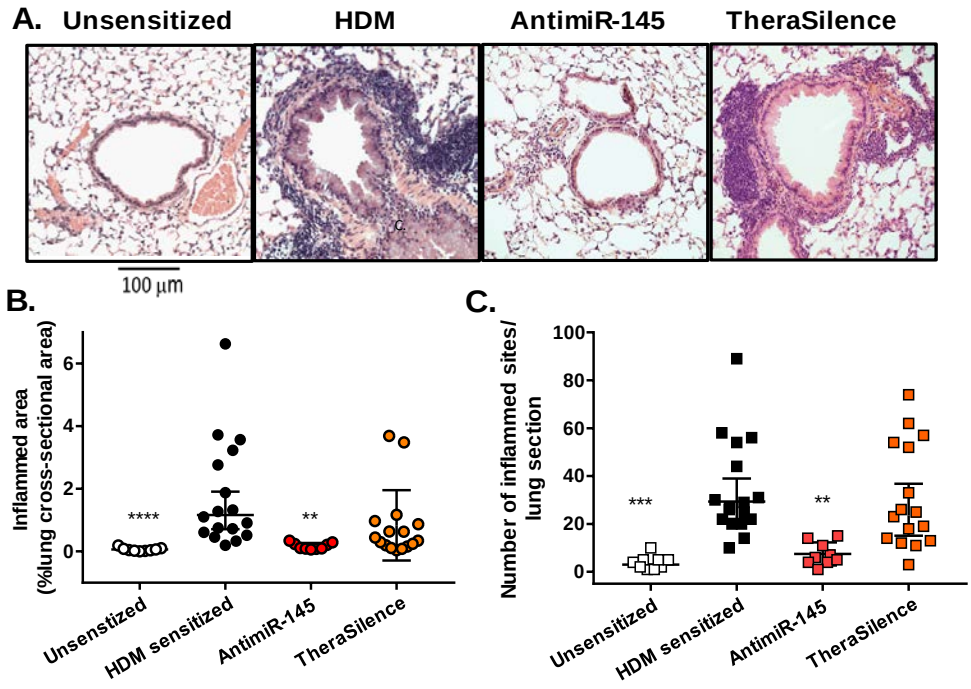

Figure S3. TheraSilence lipid nanoparticle does not have significant effects on airway inflammation. Paraffin embedded lung tissues were stained with (A) Hematoxylin and Eosin to identify inflammation (purple clusters). A representative micrograph for each treatment group was selected from all the airways within the treatment group. Images of Unsensitized , HDM-sensitized and antimiR145 treated lungs are duplicates of samples in Figure 6 used as reference images. (B) Volume density was quantified by inflammation area morphometry to determine differences in treatment groups. Data for Unsensitized, HDM and AntimiR-145 groups are reproduced from Figure 3A. (C) Number of inflamed sites in each treatment group. All numerical data are geometric mean ± 95% confidence interfavs. Hypothesis testing was conducted by Kruskal-Wallace ANOVA and Dunn's test using HD-sensitized mice as reference group; ** $p<0.005$, *** $p<0.0001$, N = 10-18.

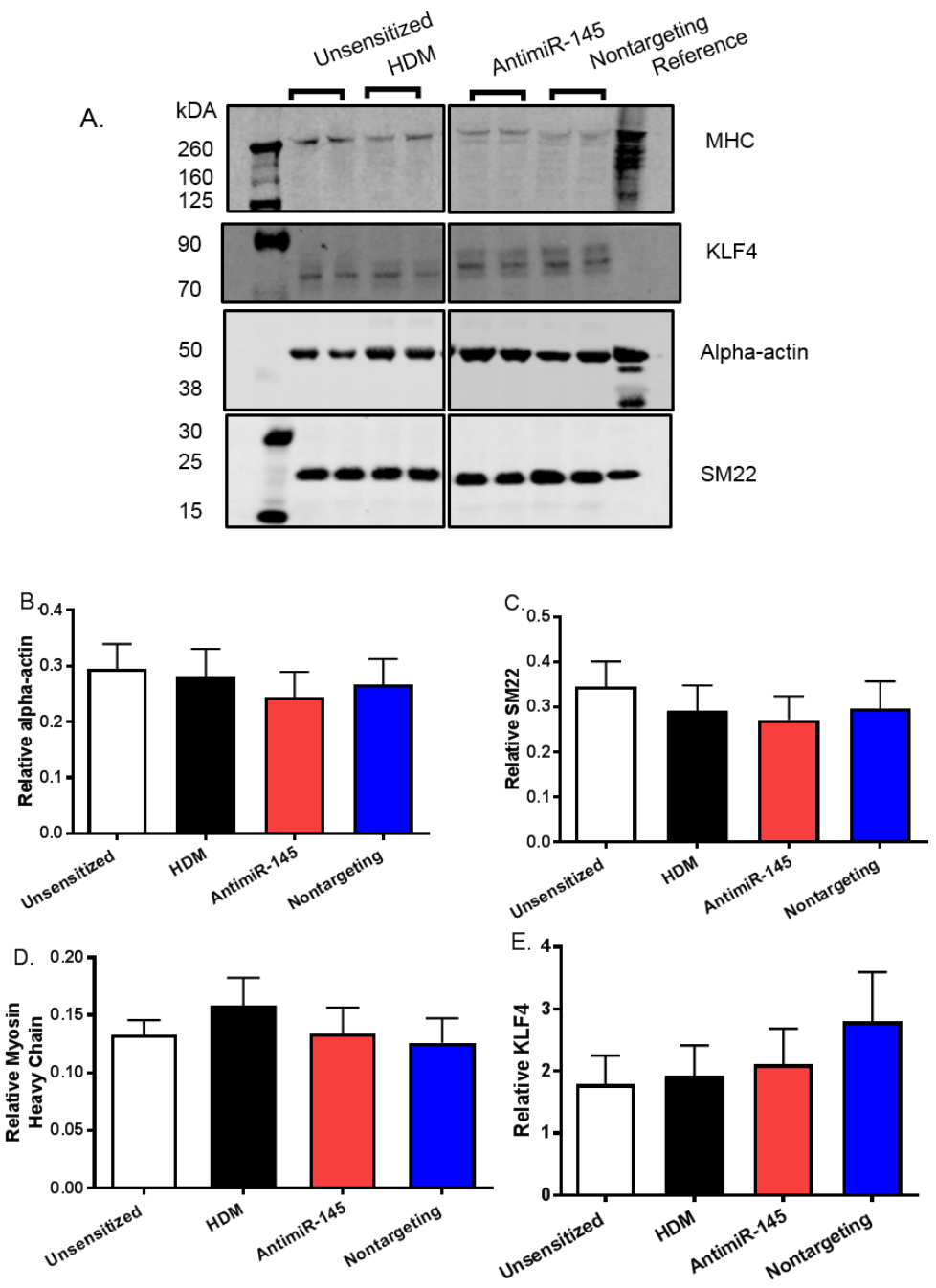

Figure S4. AntimiR-145 does not affect smooth muscle contractile protein abundance in the lung. Representative Immunoblots of protein from the lungs of mice were probed for contractile proteins (A). Quantitation of immunoblots for contractile proteins in all mice: (B) alpha-actin, (C), SM22, (D), myosin heavy chain, MHC and (E) KLF4. Human tracheal smooth muscle extract was used as a reference for quantitation. Results are mean ± SEM. Statistical analyses was performed by One-way ANOVA with Dunnett's post hoc test, * $p \leq 0.05$ comparing HDM vs antimiR-145 and HDM vs saline. N 10-11.

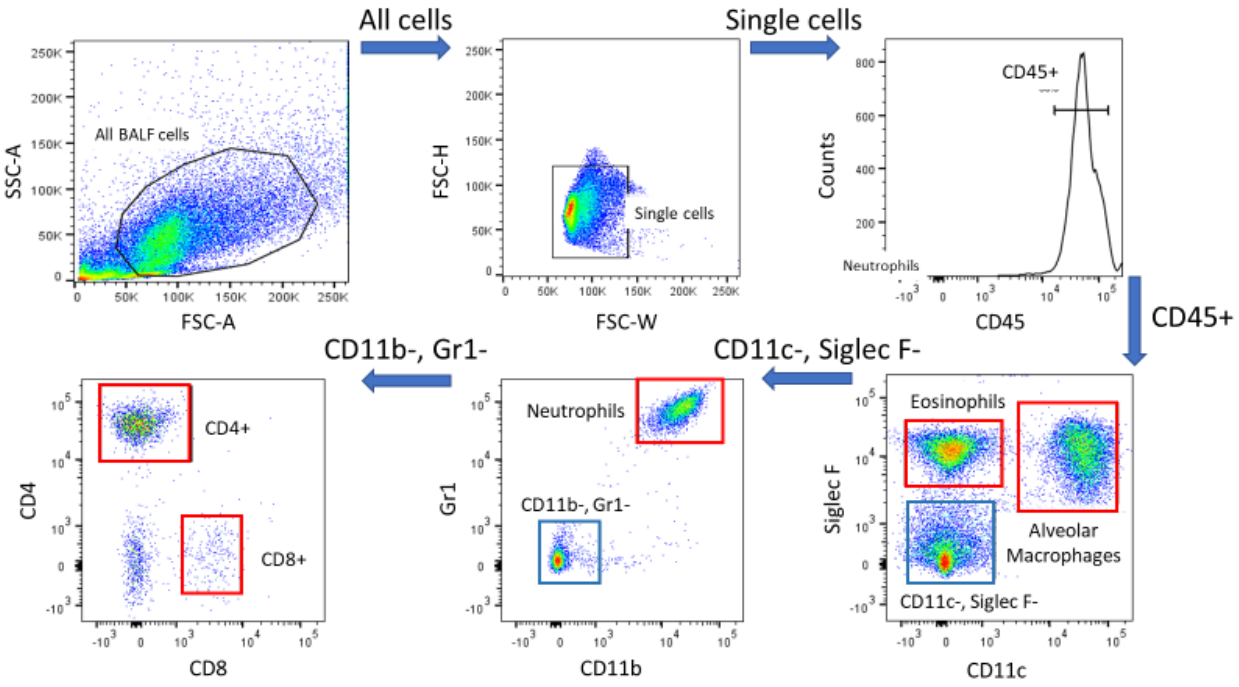

Figure S5. Gating scheme to identify cells in the bronchoalveolar lavage. Red gates indicate a terminal gate (cell population). Blue gates indicate non-terminal populations further gated as indicated by the labeled arrow of corresponding color.

Table S1. Antibodies and conjugates used in the BAL cell staining cocktail.

Target	Clone	Conjugate	Company
Fc Receptor	2.4G2	----	Bio X Cell, Lebanon, NH, USA
CD11b	M1/70	Pac Blue	BD Biosciences, San Jose, CA, USA
CD11c	N418	Brilliant Violet	Biolegend, San Diego, CA, USA
Gr1	RB6-8C5	FITC	BD PHarmigen, BD Biosciences
CD45	30-F11	PE	BD Biosciences
CD4	Gk1.5	PE-Cy7	eBiosciences, San Diego, CA, USA
CD8	53-6.7	APC-Cy7	BD Biosciences
CD68	FA-11	PerCP-Cy5.5	Biolegend
Siglec F	E50-2440	APC	BD Biosciences

Table S2. Antibodies and conjugates used in the compensation controls.

Target	Clone	Conjugate	Company
B220	R43-6B2	Pac Blue	BD Pharmigen
B220	R43-6B2	SA-Amcyan	BD Biosciences
B220	R43-6B2	FITC	eBiosciences
B220	R43-6B2	PE	BD Pharmigen
CD19	eBio 103	PE-Cy7	eBiosciences
CD19	1D3	APC-Cy7	BD pharmigen
B220	R43-6B2	PerCP-Cy5.5	eBiosciences
B220	----	APC	BD Pharmigen

Table S3. Primers used in RT-PCR and accession numbers of RT-PCR targets

mRNA	Forward (F)	Tm (°C)	Reverse (R)	Tm (°C)
Muc5ac	CAA CCT CCT CTC TTG ACA AC	54.81	GGC GAC TGG TGC TAT T	55.06
Muc5b	CCT CAA GAC CTC ATA CC	55.13	GTC CAA AGT CCA CAT TAC	55.13
IL-4	GAC GGC ACA GAG CTA TTG AT	54.78	CTC ACT CTC TGT GGT CTT C	62
IL-5	TGA AGT GCT GGA GAT GGA AC	54.72	GCT AGG AGA AAG GAT GCT AAG G	54.78
IL-13	GGA TTC CCT GAC CAA CAT CTC	55.19	AGG GAT GGT CTC TCC TCA TT	54.87
IL-17a	CAA CCT CCT CTC TTG ACA CTA AC	54.81	GGC GAC TGG TGC TGA TAT T	55.06
Eotaxin-1	GCA GCA TGG TAT GGA GTG T	55.08	TAT CCT CTG GGT CCT GTA GAT G	54.96
Hprt	CCC CAA AAT GGT TAA GGT TGC	54.76	AAC AAA GTC TGG CCT GTA TCC	54.86
	Ensembl Gene ID			
Muc5ac	ENSMUSG00000037974			
Muc5b	ENSMUSG00000066108			
IL-4	ENSMUSG00000000869			
IL-5	ENSMUSG00000036117			
IL-13	ENSMUSG00000020383			
IL-17a	ENSMUSG00000025929			
Eotaxin-1	ENSMUSG00000020676			
Hprt	ENSMUSG00000025630			

Table S4. Validated miR-145 targets and functions relevant to lung remodeling

Cell type	Targets	Functional effect	Reference
Smooth muscle	KLF4/5 Fascin	↑ contractile proteins ↓ proliferation and motility	46 66 67
Endothelial cells	JAM-A	↓atherosclerotic lesions	68
Epithelial cells	CFTR	↓CFTR protein	69 70
Immune cells	PDE8A (macrophages) PBMCs CTLA-4 (Treg)	Modifies HIV replication ↑cell content of miR-145 Undefined	71 72 73
Stem cells	OCT4, SOX2, KLF4 Dab2	↓pluripotency ↓Wnt/β catenin activity	74, 75